



James S. Cohen and John D. Morgan III

## Contents

91.1	<b>Introduction</b> . . . . .	1359
91.2	<b>Nuclear Size Effects in Atoms</b> . . . . .	1360
91.2.1	Nuclear Size Effects on Nonrelativistic Energies . . . . .	1360
91.2.2	Nuclear Size Effects on Relativistic Energies . . . . .	1361
91.2.3	Nuclear Size Effects on QED Corrections . . . . .	1362
91.3	<b>Electronic Structure Effects in Nuclear Physics</b> . . . . .	1362
91.3.1	Electronic Effects on Closely Spaced Nuclear Energy Levels . . . . .	1362
91.3.2	Electronic Effects on Tritium Beta Decay . . . . .	1362
91.3.3	Electronic Screening of Low-Energy Nuclear Reactions . . . . .	1362
91.3.4	Atomic and Molecular Effects in Relativistic Ion–Atom Collisions . . . . .	1363
91.4	<b>Muon-Catalyzed Fusion</b> . . . . .	1363
91.4.1	The Catalysis Cycle . . . . .	1365
91.4.2	Muon Atomic Capture . . . . .	1365
91.4.3	Muonic Atom Deexcitation and Transfer . . . . .	1367
91.4.4	Muonic Molecule Formation . . . . .	1368
91.4.5	Fusion . . . . .	1370
91.4.6	Sticking and Stripping . . . . .	1370
91.4.7	Prospectus . . . . .	1372
	<b>References</b> . . . . .	1372

## Abstract

For an atom with a small to moderately large atomic number  $Z$ , the typical length scale  $a_0/Z$  of the innermost core orbitals is so much larger than typical nuclear length scales that the corrections to the energy levels and wave functions arising from the nonzero electric charge radius of the nucleus can accurately be computed using first-order perturbation theory, as is described in Sect. 91.2.

J. S. Cohen (✉)  
Atomic and Optical Theory, Los Alamos National Laboratory  
Los Alamos, NM, USA  
e-mail: cohen@mailaps.org

J. D. Morgan III  
Dept. of Physics & Astronomy, University of Delaware  
Newark, DE, USA  
e-mail: jdmorgan@udel.edu

Nonetheless, these relatively small shifts can sometimes have a profound effect on processes in atomic and/or nuclear physics, particularly if two or more energy levels are very close. For example, as is discussed in Sect. 91.3, the presence of the electron cloud makes energetically possible the  $\beta$ -decay of  $^{187}\text{Re}$  to  $^{187}\text{Os}$  and significantly modifies the energy distribution of products in the  $\beta$ -decay of tritium in various chemical environments. Also, electronic screening can greatly enhance the cross sections of low-energy nuclear reactions relative to what they would be for bare nuclei.

In isotopes of hydrogen, the replacement of an electron by a muon, with  $m_\mu \approx 207m_e$ , results in a tiny neutral *atom* that can closely approach another nucleus, thereby catalyzing nuclear fusion. For example, the rate of deuterium–tritium fusion is enhanced by 77 orders of magnitude if a single electron is replaced by a muon. A rich variety of bound-state properties and scattering processes for these exotic atoms and molecules has been extensively investigated, as is reviewed in Sect. 91.4.

## Keywords

muonic atom · sticking probability · muon transfer · muonic molecule · molecular wave function

## 91.1 Introduction

That nuclei are not infinitesimally small, structureless particles causes small but perceptible shifts in the electronic structure of atoms and molecules. Even for nuclei with a small atomic number  $Z$ , the effects are readily detectable through modern high-precision spectroscopy, and their magnitude grows as  $Z^{14/3}$ . Conversely, the presence of electrons tightly bound to atomic nuclei can alter the ordering of nuclear energy levels or make them unstable to  $\beta$  decay. Atomic effects can also influence nuclear branching ratios into the product

channels. Nominally small atomic effects have been shown to affect the complicated chain of nuclear reactions responsible for the generation of energy in the sun. Setting bounds to the rest mass of the neutrino from the endpoint of the  $\beta$ -decay spectrum of tritium requires a precise understanding of atomic and molecular structure and scattering processes.

The great disparity between nuclear scales of energy (several MeV) and distance ( $10^{-5}$  to  $10^{-4}$  Å) and the corresponding atomic scales (several eV and 1 Å, respectively) usually allows the separate treatment of nuclear and atomic effects. However, since not absolute energies but energy differences determine the magnitudes of perturbative effects, near coincidences in energy differences can greatly enhance the interplay between the two regimes. Such comparable differences of energies account for the important role of nuclear structure in the Lamb shift splitting between the  $2s_{1/2}$  and  $2p_{1/2}$  states of the hydrogen atom (Chap. 28) and the influence of atomic structure on nuclear processes (Sects. 91.2 and 91.3).

For the case of muonic atoms and molecules, the interplay is enhanced by the much larger mass of a muon relative to an electron. This decreases the distance scale by a factor of  $m_e/m_\mu$  and increases the energy scale by a factor of  $m_\mu/m_e$ . Small corrections such as the vacuum polarization part of the Lamb shift are amplified even more ( $\approx (m_\mu/m_e)^3$  for low  $Z$ ).

Besides the areas where atomic physics effects play an important role in nuclear physics, or vice versa, it is worth remembering that atomic and molecular physicists and nuclear physicists can benefit from knowing the theoretical techniques that have been developed in each others' fields. For example, it is well known that group theoretical methods are widely employed in formulating and solving many-body problems in nuclear, atomic, and molecular physics. To take another case, the coupled-cluster method, which was first proposed in the late 1950s by *Coester* and *Kümmel* in the context of nuclear theory [1–3], was applied a decade later to electronic structure problems in atomic and molecular physics and quantum chemistry by *Cizek*, *Paldua*, and *Shavitt* [4–6], and in the 1980s was widely developed by Rod Bartlett and coworkers at the University of Florida and by John Pople and coworkers at Carnegie Mellon University. *Quantum halos*, which are very loosely bound states for which most of the probability density is spread diffusely over the classically forbidden region, have been treated in a unified manner for both nuclear and molecular systems [7].

## 91.2 Nuclear Size Effects in Atoms

### 91.2.1 Nuclear Size Effects on Nonrelativistic Energies

Interest in the influence of a finite nuclear charge distribution on the energy levels of the hydrogen atom goes back

to the measurement of the Lamb shift [8–11], and to even earlier indications that the fine structure of hydrogen did not quite agree with the predictions of the Dirac equation for a point nucleus [12–15]. The finite proton size does, in fact, raise the energy of the  $2s_{1/2}$  state relative to  $2p_{1/2}$ , but the shift is only  $\approx 0.012\%$  of the dominant electron self-energy contribution (Chap. 28). It must nevertheless be taken into account in high-precision tests of QED. A long-standing disagreement in the proton size between values obtained from electron-based measurements and muon-based measurements has now been resolved [16], resulting in the value  $r_p = 0.833(10)$  fm, in excellent agreement with the muonic value  $r_p = 0.84087(39)$  fm [17, 18].

Early derivations were given by several authors [19–22] and generalized by *Zemach* [23] (also [24]) to a form involving integrals over the nuclear electric and magnetic form factors. The basic result is illustrated by the following argument. Let  $\rho(\mathbf{r})$  be the electron density, which may have no spatial symmetry properties in the particular case of a polyatomic molecule, and  $\rho_n(\mathbf{r}_n)$  be the charge density of a nucleus, which obeys

$$\int d^3r_n \rho_n(\mathbf{r}_n) = Z. \quad (91.1)$$

Assume that  $\rho_n(\mathbf{r}_n)$  has no permanent electric dipole moment, so that

$$\int d^3r_n \mathbf{r}_n \rho_n(\mathbf{r}_n) = \mathbf{0}. \quad (91.2)$$

By writing the Coulomb potential for a point-like nucleus as

$$-\frac{Z}{r} = -\int d^3r_n \frac{Z\delta^{(3)}(\mathbf{r}_n)}{|\mathbf{r} - \mathbf{r}_n|}, \quad (91.3)$$

the first-order shift of the electronic energy due to the replacement of the point-like nucleus by an extended nucleus is

$$\Delta E_{\text{nuc}} = \int d^3r \int d^3r_n \frac{Z\delta^{(3)}(\mathbf{r}_n) - \rho_n(\mathbf{r}_n)}{|\mathbf{r} - \mathbf{r}_n|} \rho(\mathbf{r}). \quad (91.4)$$

Since the Fourier transform, defined by

$$\hat{\rho}_n(\mathbf{k}) = \int d^3r_n e^{-i\mathbf{k}\cdot\mathbf{r}_n} \rho_n(\mathbf{r}_n), \quad (91.5)$$

preserves inner products within a factor of  $(2\pi)^3$  and maps convolutions to simple products, the integral in Eq. (91.4) reduces to

$$(2\pi)^3 \int d^3k [Z - \hat{\rho}_n(\mathbf{k})] \frac{4\pi}{k^2} \hat{\rho}(\mathbf{k}), \quad (91.6)$$

where the hats denote the Fourier transforms of the densities, and  $4\pi/k^2$  is the Fourier transform of the Coulomb potential  $1/r$ . Since  $Z = \int d^3r_n \rho_n(\mathbf{r}_n)$ , the energy shift can be

reexpressed as

$$(2\pi)^3 \int d^3k \int d^3r_n (1 - e^{-i\mathbf{k}\cdot\mathbf{r}_n}) \rho_n(\mathbf{r}_n) \frac{4\pi}{k^2} \hat{\rho}(\mathbf{k}), \quad (91.7)$$

which is still an exact first-order perturbation expression. Since typical nuclear length scales are much smaller than typical nonrelativistic atomic length scales, it is legitimate to expand the exponential in a Taylor series. The zeroth-order term,  $-1$ , is canceled by the  $+1$ . The linear term,  $i\mathbf{k}\cdot\mathbf{r}_n$ , contributes nothing by the hypothesis that the nuclear charge distribution has no permanent electric dipole moment. The first nonvanishing term is

$$(2\pi)^3 \int d^3k \int d^3r_n \frac{1}{2}(\mathbf{k}\cdot\mathbf{r}_n)^2 \rho_n(\mathbf{r}_n) \frac{4\pi}{k^2} \hat{\rho}(\mathbf{k}). \quad (91.8)$$

If  $\rho(\mathbf{r})$  is nonzero at the nucleus, then for large  $k$ , the leading behavior of  $\hat{\rho}(\mathbf{k})$  is that of a spherically symmetric  $s$ -wave with a radial dependence proportional to  $k^{-4}$ . The angular integration in the variable  $\mathbf{k}$  leads to the replacement of  $(\mathbf{k}\cdot\mathbf{r}_n)^2$  by its average value  $(1/3)k^2r_n^2$ , so the expression Eq. (91.8) reduces to

$$\frac{2\pi}{3} (2\pi)^3 \int d^3k \hat{\rho}(\mathbf{k}) \int d^3r_n r_n^2 \rho_n(\mathbf{r}_n), \quad (91.9)$$

which can be further simplified by observing that

$$(2\pi)^3 \int d^3k \hat{\rho}(\mathbf{k}) = (2\pi)^3 \int d^3k e^{i0\cdot\mathbf{k}} \hat{\rho}(\mathbf{k}) = \rho(0), \quad (91.10)$$

and by definition

$$\int d^3r_n r_n^2 \rho_n(\mathbf{r}_n) = Z\langle r_n^2 \rangle, \quad (91.11)$$

thus yielding the final expression

$$\Delta E_{\text{nuc}} = \frac{2\pi}{3} Z e^2 \rho(0) \langle r_n^2 \rangle, \quad (91.12)$$

with

$$\rho(0) = \left(\frac{\mu}{m_e}\right)^3 \frac{Z^3}{\pi n^3} a_0^{-3} \quad (91.13)$$

for a hydrogenic ion with reduced mass  $\mu$ . This derivation is independent of the specific nuclear model or the assumption of spherical symmetry of the electron density. Since  $\langle r_n^2 \rangle$  scales as  $Z^{2/3}$ ,  $\Delta E_{\text{nuc}}$  then scales as  $Z^{14/3}$ . For a molecule with several nuclei, the contributions Eq. (91.12) from each nucleus should be summed.

For the helium atom,  $\rho(0) = \langle \delta(\mathbf{r}_1) + \delta(\mathbf{r}_2) \rangle$  can be accurately calculated from high-precision variational wave functions (Chap. 12). For the  $1s_2 \ ^1S_0$  ground state,  $\rho(0) \simeq$

$(\mu/m_e)^3 [3.6208586 - 0.18237(\mu/M)] a_0^{-3}$ , where  $M$  is the nuclear mass. Results for other states up to  $n = 10$  are tabulated in [25]. Combined with high-precision isotope shift measurements, the results can be used to extract differences in nuclear radii for pairs such as  $^3\text{He}/^4\text{He}$ ,  $^6\text{Li}/^7\text{Li}$ , and  $\text{H}/\text{D}$  [26–29]. The method has been applied to the short-lived, neutron-rich nuclei  $^6\text{He}$ ,  $^8\text{Li}$ , and  $^9\text{Li}$  [30, 31].

Equation (91.12) works well for atoms with small  $Z$ , since relativistic corrections to the electron density are small. However, it breaks down for heavier nuclei, for which relativistic wave functions are needed.

## 91.2.2 Nuclear Size Effects on Relativistic Energies

The preceding analysis breaks down for relativistic wave functions because they are singular at a point nucleus, making  $\rho(\mathbf{0})$  infinite. In this case, the Dirac equations with Hamiltonians  $H_0$  and  $H$  for the point nucleus and distributed nucleus cases, respectively, can be combined to obtain

$$(E - E_0)\Psi^\dagger\Psi_0 = \Psi^\dagger H\Psi_0 - \Psi^\dagger H_0\Psi_0. \quad (91.14)$$

If a finite radius  $r_s$  is now chosen such that  $H = H_0$  outside the sphere  $r = r_s$ , then this equation can be integrated from  $r_s$  outward to yield [32]

$$\Delta E_{\text{nuc}} = \frac{\hbar c (gf_0 - fg_0)_{r=r_s}}{\int_{r_s}^{\infty} (gg_0 + ff_0) dr}, \quad (91.15)$$

where  $f_0$  and  $f$  are the large radial components of  $\Psi_0$ , and  $\Psi$  and  $g_0$  and  $g$  are their small radial components (Chap. 9), and the numerator is the surface term that remains after integrating by parts the  $c\boldsymbol{\alpha}\cdot\mathbf{p}$  term in  $H$ . The units are  $\hbar c/a_0 = \alpha m_e c^2$ . The solutions can be further expanded in terms of Bessel functions, or the Dirac equation can simply be integrated numerically.

For hydrogenic ions up to moderately large  $Z$ , the results are reasonably well represented by [33, 34]

$$\Delta E_{\text{nuc}} = \frac{2}{3n^3} (Z\alpha)^2 m_e c^2 \times [\delta_{\ell,0} + C_2(Z\alpha)^2] (Z^2 \langle r_n^2 \rangle / a_0^2)^\gamma, \quad (91.16)$$

with  $\gamma = [1 - (Z\alpha)^2]^{1/2}$ , and  $C_2 \simeq 0.50, 1.38$ , and  $0.1875$  for the  $1S_{1/2}$ ,  $2S_{1/2}$ , and  $2P_{1/2}$  states, respectively. Extensions to higher-order terms are discussed in [35]. The above formula was used in the tabulations of *Mohr* [34] for  $10 \leq Z \leq 40$ , while *Johnson* and *Soff* [36] used the numerical integration method for  $Z$  up to 110. The nuclear electric and magnetization density distributions are tabulated in [37], nuclear moments in [38], and nuclear masses in [39]. In the absence

of better data, the root-mean-square nuclear radius can be estimated from  $\langle r_n^2 \rangle^{1/2} \approx 0.777A^{1/3} + 0.778 \pm 0.06$  fm, where  $A$  is the atomic mass number.

### 91.2.3 Nuclear Size Effects on QED Corrections

The progress in the experimental study of transition energies in heavy ions stripped of most of their electrons [40–42] has inspired theoretical work on modifications of QED corrections due to an extended nuclear charge distribution. Calculations based on propagators expanded in terms of basis splines [43–45] (Sect. 8.1.1) have led to relatively rapid convergence with the number of angular functions.

## 91.3 Electronic Structure Effects in Nuclear Physics

### 91.3.1 Electronic Effects on Closely Spaced Nuclear Energy Levels

The presence of a nearby cloud of electrons can significantly affect nuclear processes involving closely spaced nuclear energy levels. One of the most dramatic cases involves the  $\beta$ -decay process  $^{187}\text{Re} \rightarrow ^{187}\text{Os} + e^- + \bar{\nu}_e$ , which is energetically forbidden by about 12 keV for bare nuclei but becomes allowed for the neutral atoms when the difference in electronic binding energies is included. The nuclear charges are  $Z = 75$  for  $^{187}\text{Re}$  and  $Z = 76$  for  $^{187}\text{Os}$ . There is also the possibility of the electron being captured into a bound state of  $^{187}\text{Os}$ , as opposed to the continuum  $\beta$ -decay process.

The total electronic binding energies of heavy neutral atoms can be roughly estimated using the large- $Z$  expansion for  $E(Z)$  given by Eq. (21.31) in Chap. 21. The difference between the energies of two neutral atoms with atomic numbers  $Z + 1$  and  $Z$ , respectively, is then given approximately by

$$\begin{aligned} E(Z + 1) - E(Z) &\simeq \frac{dE}{dZ} \\ &\simeq (-48.83Z^{4/3} + 27.21Z^{3/3} \\ &\quad - 12.24Z^{2/3}) \text{ eV}, \end{aligned} \quad (91.17)$$

which amounts to about  $-13.6$  keV at  $Z = 75$ . This is sufficient to overcome the 12 keV energy deficit in the otherwise energetically forbidden  $\beta$ -decay of  $^{187}\text{Re}$ .

The general theory of bound state  $\beta$ -decay is discussed by *Bahcall* [46], who also calculated the ratio  $\rho$  of bound state  $\beta$ -decay to continuum  $\beta$ -decay for bare nuclei. In the case of  $^{187}\text{Re} \rightarrow ^{187}\text{Os}$ ,  $\rho$  is of importance in estimating changes in the half-life for  $\beta$ -decay of  $^{187}\text{Re}$  under various conditions of ionization, since the measured isotope ratios  $^{187}\text{Re}/^{188}\text{Re}$

and  $^{187}\text{Os}/^{188}\text{Os}$  from terrestrial rocks and meteorites can be used to determine not only the age of the solar system but also the age of our galaxy [47, 48]. Estimates based on a modified Thomas–Fermi (TF) model [49] indicate that  $\rho \simeq 0.01$ , and further multiconfiguration Dirac–Fock calculations give  $\rho = 0.005$  to  $0.007$  [50–52]. See [50–52] for further details and references.

### 91.3.2 Electronic Effects on Tritium Beta Decay

The mass of the neutrino, normally taken to be zero in the Standard Model, can be determined in principle from analysis of the  $\beta$ -decay process  $^3\text{T} \rightarrow ^3\text{He}^+ + e^- + \bar{\nu}_e$ . An early measurement based on this method [53–55] yielded a neutrino mass of  $\approx 25$  eV. Several independent tests of this result were initiated soon thereafter. Since the experiments are performed not on bare tritons but on tritium gases and solids under various conditions, it is essential to understand quantitatively the atomic and molecular processes that affect the distribution of the highest-energy electrons produced from various initial states [56, 57].

*Martin* and *Cohen* [58] used a Stieltjes imaging technique to calculate shakeup and shakeoff probabilities for the  $\beta$ -decay of  $\text{T}_2$  into  $^3\text{HeT}^+$ . Simultaneously, extensive calculations were carried out by *Kolos*, *Jeziorski*, *Szalewicz*, *Monkhorst*, et al. [59–63] using potential energy curves for the reactant  $\text{T}_2$  and  $\text{TH}$  molecules and the product  $^3\text{HeT}^+$  and  $^3\text{HeH}^+$  molecules and accounting for the production of electronically and rovibrationally ground and excited final states, as well as resonant states. Nuclear motion was found to have a small but detectable effect on the results, and solid-state effects for frozen  $\text{T}_2$  were also investigated and found to be small. These calculations played a crucial role in the interpretation of the experiments [64–68], which indicated that the neutrino mass is less than  $\approx 10$  eV. In 1998, there was published evidence from the super-Kamiokande experiment that the three flavors of neutrinos oscillate, as further confirmed by the Sudbury Neutrino Observatory. This implies that neutrinos have a nonzero rest mass [69]. Subsequently, upper bounds of the order of a few eV to the neutrino mass have been derived from measurements of tritium beta decay [70, 71] and from cosmological considerations [72]. As of 2018 the best upper bound from tritium beta decay experiments was about 2 eV [73].

### 91.3.3 Electronic Screening of Low-Energy Nuclear Reactions

The cross section  $\sigma(E)$  for a nuclear reaction involving charged reactants drops very rapidly for collision energies  $E$  below the Coulomb barrier. A WKB treatment shows that

for low collision energies, the dependence of  $\sigma(E)$  can be conveniently expressed as

$$\sigma(E) = S(E) E^{-1} e^{-2\pi\eta}, \quad (91.18)$$

where  $S(E)$  is the astrophysical factor, and

$$\eta = Z_1 Z_2 \alpha c (\mu/2E)^{1/2} \quad (91.19)$$

is the Sommerfeld parameter, which depends on the charge numbers  $Z_1$  and  $Z_2$  of the projectile and target nuclides, their reduced mass  $\mu$ , and the center-of-mass energy  $E$ . For nuclear reactions involving light nuclei, it is found that  $S(E)$  typically varies slowly with  $E$  except close to resonances. Thus, an accurate determination of  $S(E)$  at moderately low  $E$  can be used to extrapolate  $\sigma(E)$  to much lower energies, which are beyond the reach of laboratory experiments but are of great relevance to the nuclear reactions that occur in stars.

However, electron screening effects can greatly enhance cross sections for nuclear reactions as measured in the laboratory at low energy [74], because at least the target nucleus is almost always surrounded by a cloud of electrons that screen the Coulomb repulsion between nuclei. The effect has been observed in various low-energy reactions such as  ${}^3\text{He}(d, p){}^4\text{He}$ ,  ${}^6\text{Li}(p, \alpha){}^3\text{He}$ ,  ${}^6\text{Li}(d, \alpha){}^4\text{He}$ , and  ${}^6\text{Li}(p, \alpha){}^4\text{He}$  [75–78]. Since reactions in stars involve bare nuclei, the laboratory data must be carefully corrected for screening effects.

Analysis of the data for the  ${}^3\text{He}(d, p){}^4\text{He}$  reaction indicates that the effect of screening is always greater than that predicted in the adiabatic limit [79–81]. A more general theoretical treatment of the  $d + {}^2\text{H}$  and  $d + {}^3\text{He}$  reactions [82], using a time-dependent Hartree–Fock method for the electrons screening and classical motion for the nuclei found less enhancement than that observed. An improved treatment taking account of electron correlation and quantum-mechanical effects on the nuclear motion will likely be needed. This remains an important area of development for the future.

For some work on the subject of electronic screening of low-energy nuclear reactions, see [83–88].

### 91.3.4 Atomic and Molecular Effects in Relativistic Ion–Atom Collisions

High-energy accelerators can now produce beams of atomic ions partly or completely stripped of their electrons, even for  $Z$  as high as 92. The collisions of such beams of highly charged ions with fixed targets involve a broad array of atomic and molecular processes, such as excitation, ionization, charge transfer, and, in the extreme relativistic case, pair production. A similarly broad array of theoretical techniques is required to study these topics. A thorough review of these,

including comparisons with experimental data where available, is given in [89, 90].

A topic of particular interest is the first experimental observation of the capture of electrons from electron–positron pair production in the extreme relativistic collision of a 0.96 GeV/nucleon  $\text{U}^{92+}$  beam with gold, silver, copper, and Mylar targets [91]. The energy and angular distributions of the positrons were also measured. For the gold target, the cross section for capture was nearly as large as that for pair production without capture, and it was found to vary with the nuclear charge  $Z_t$  of the target nucleus roughly as  $Z_t^{2.8(\pm 0.25)}$ . Neither the dependence on  $Z_t$  nor the relatively great probability for capture is in agreement with perturbation theory, which highlights the need for further exploration of this exotic system.

## 91.4 Muon-Catalyzed Fusion

Exotic muonic atoms and molecules are more suitable subjects than electronic atoms and molecules for probing some physical effects. The muon  $\mu^-$  is a leptonic elementary particle like the electron, except that it is 206.768 times more massive and has a finite lifetime ( $\tau_0 = 1/\lambda_0$ , where  $\lambda_0$  is the rate of decay) of 2.197  $\mu\text{s}$ . This lifetime is amply long for most experiments. In normal atoms, the fine-structure splitting (due to  $\mathbf{L} \cdot \mathbf{S}$  coupling) is much larger than the hyperfine splitting (due to  $\mathbf{s}_{\text{nuc}} \cdot \mathbf{s}_e$  coupling); this relation is reversed in muonic atoms. Likewise, vacuum polarization, relativistic, finite-nuclear-size, and nonadiabatic effects are enhanced. (Note: the muonic Bohr radius  $\hbar^2/m_\mu e^2 \approx (1/207) a_0$  is similar in size to the Compton wavelength  $\hbar/m_e c \approx (1/137) a_0$ .) Remarkably, muonic molecules make nuclear fusion possible at room temperature. In the phenomenon of muon-catalyzed fusion ( $\mu\text{CF}$ ), there are both indirect and direct interactions between the atomic and molecular physics and the nuclear physics. Indirectly, the atomic and molecular densities and transition rates control the nuclear fusion rates, and, in turn, the kinetic energies of the fusion products affect the atomic and molecular kinetics. Directly, the nuclear structure affects some molecular energy levels that determine important resonant rates and the boundary condition on the muonic wave functions used to calculate the muon *sticking* loss.

The phenomenon of  $\mu\text{CF}$  was actually discussed theoretically [92–94] before it was experimentally observed [95]. Shortly after its observation, its possible use for energy production was discussed [96]. This was an attractive prospect, since hot fusion schemes are made difficult by the electrostatic (Coulomb) repulsion between nuclei. In the two conventional approaches to controlled fusion, magnetic and inertial confinement, this barrier is partially surmounted by energetic collisions. (Note: the particle densities  $N$  and con-

finement times  $\tau$  in the hot plasmas ( $T \gtrsim 10^8$  K) are typically more than ten orders of magnitude different for these two schemes, but the product of the two required for d-t fusion is  $N\tau \gtrsim 10^{14}$  s/cm<sup>3</sup> in either case. For muon-catalyzed fusion, effectively  $N\tau \approx 10^{25}$  s/cm<sup>3</sup>, but this criterion does not tell the real story.) In contrast, in  $\mu$ CF, the objective is for the nuclei to tunnel through the barrier without the benefit of kinetic energy. This feat is enabled by binding two hydrogenic nuclei (p, d, or t) in an exotic molecule like  $H_2^+$  with the electron replaced by a negative muon.

Since the molecular size is inversely proportional to the mass of the binding particle, the average distance between nuclei in  $pp\mu$  is  $\approx 1/200$  Å (500 fm) instead of 1 Å as in  $ppe$  (i.e.,  $H_2^+$ ). This distance, which would be reached in a d + d collision at  $\approx 3$  keV ( $\approx 3 \times 10^7$  K), is still large compared with the separation of a few fm where the nuclear strong forces cause fusion, but fusion occurs rapidly because of the increased vibrational frequency and, more importantly, the increased probability of tunneling per vibration. The vibrational frequency is  $(m_\mu/m_e)^{3/2} \approx 3 \times 10^3$  times faster than for the corresponding electronic molecule. (Note: for comparison, the muonic/electronic energy scales as  $m_\mu/m_e$  and the rotational energy scales as  $(m_\mu/m_e)^2$ . These relations [97] are based on the Born–Oppenheimer approximation, which is not very accurate for muonic molecules.) The effect on the tunneling probability depends on the nuclear masses; for  $dt\mu$ , which has the largest nuclear matrix element (astrophysical  $S$  factor, Sect. 91.3.3), the increase is by a factor of  $\approx 10^{77}$  compared with DT, and the consequential fusion rate is  $\lambda_{dt\mu}^f \approx 10^{12}$  s<sup>-1</sup>.

Just on the basis of the fusion rate, one would expect a yield of  $\lambda_{dt\mu}^f/\lambda_0 \approx 10^6$  muon-catalyzed d-t fusions for the average muon. While this number indeed provides an upper limit, the actual average number of fusions,  $\approx 150$  for  $dt\mu$ , is much smaller and is determined by the atomic and molecular physics of the catalysis cycle (although the energy released in the nuclear fusion does play an important role here). Some of the atomic and molecular processes in the  $\mu$ CF cycle are quite ordinary, but others, like atomic capture and resonant molecular formation, have no counterpart with normal atoms.

Muon-catalyzed fusions of all pairs of hydrogen isotopes, except two protons, have been observed. Based on the experiments and theory, the dominant reaction products are [98–103]:

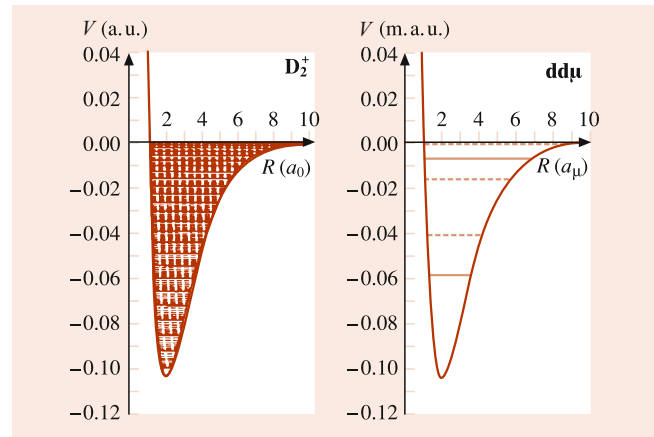
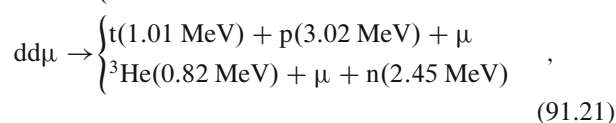
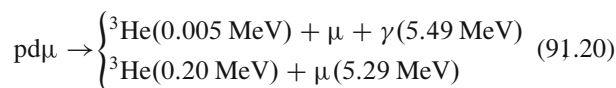
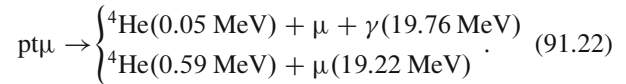
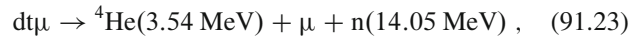


**Fig. 91.1** Rovibrational energy levels for  $D_2^+$  and  $dd\mu$ . The  $J = 0$  levels are shown as solid lines, and the  $J > 0$  levels are shown as dashed lines. For  $D_2^+$ , all 28 vibrational levels are displayed, but the associated rotational levels are displayed only up to the next higher vibrational level. All levels of  $dd\mu$  are displayed; the  $(J = 1, v = 1)$  level is barely discernible below the  $V = 0$  axis



(Note: A channel producing  ${}^4\text{He}$  and a  $e^+e^-$  pair was theoretically predicted to be significant [104] but seems to be ruled out by experimental results published in 2012 [105].)



In these reactions, a  $\mu$  without an energy designated is a spectator; i.e., it serves to bring the nuclei together but plays no significant role in the kinematics of the reaction – such a  $\mu$  may actually be bound (stuck) to one of the product nuclei.

Each reaction is of special interest in its own right:  $pd\mu$  and  $pt\mu$  for the contribution of  $\mu$  conversion, and  $tt\mu$  for the correlation of the two final state neutrons. Only the  $dd\mu$  and  $dt\mu$  molecular formations are resonant; i.e., their formation can occur in a one-body state because they, and only they, possess a loosely bound state such that the muonic binding energy can go into rovibrational energy of the electronic molecule. That the existence of such a state really is fortuitous can be seen in Fig. 91.1 where the bound rovibrational states of  $dd\mu$  (1 m.a.u. = 5626.5 eV) are compared with the rovibrational states of  $D_2^+$  (1 a.u. = 27.2 eV). Although both  $dd\mu$  and  $dt\mu$  can be formed resonantly,  $dt\mu$  is unique in having a rapid (as compared with muon decay) formation rate and also in having a small sticking loss. The sticking loss is due to the possibility that the negatively charged muon may form a bound state with the positively charged fusion product. The relatively low branching fraction ( $< 1\%$ ) for  $dt\mu \rightarrow {}^4\text{He}\mu + n$  is due simply to the high speed of the outgoing  ${}^4\text{He}$  ( $\alpha$  particle).

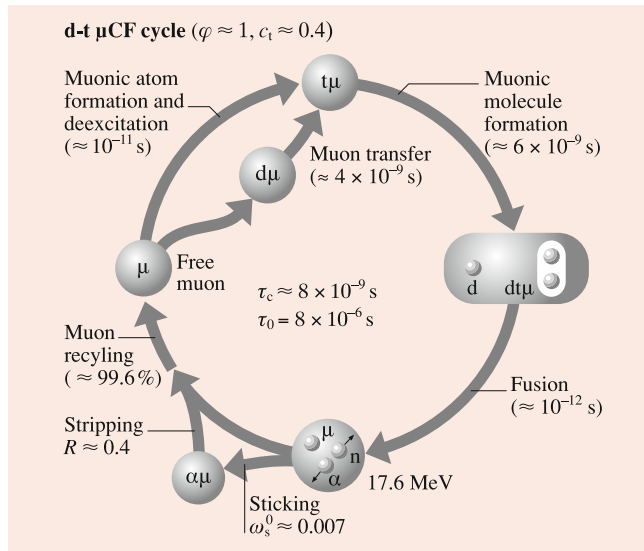


**Fig. 91.2** The simplified d-t muon-catalyzed fusion cycle. The times are for density  $\phi = 1$  (liquid hydrogen density) and tritium fraction  $c_t = 0.4$ ;  $\tau_c$  is the cycle time, and  $\tau_0$  is the muon-decay time

### 91.4.1 The Catalysis Cycle

A diagram of the  $\mu$ CF cycle for a d-t mixture is shown in Fig. 91.2. The basic steps in the cycle are

1. Atomic capture to form  $d\mu$  or  $t\mu$  (initially in a highly excited state,  $n \gtrsim 14$ ).
2. Transfer of the  $\mu$  from d to t, if necessary.
3. Resonant molecular formation, shown schematically. Here, the  $dt\mu$  is so small (in reality) that it can be considered to be a pseudo-nucleus in the electronic molecule.
4. Nuclear fusion.
5. Sticking ( $\alpha\mu$  formation) or recycling.

The reaction times shown are at liquid hydrogen density, abbreviated as LHD ( $\phi = 1$  in the conventional LHD units) and a tritium fraction  $c_t = 0.4$ , which is close to the value that maximizes the number of cycles. The times for muonic atom formation and deexcitation,  $\approx$  ps, are short compared with the times for muon transfer and molecular formation,  $\approx$  ns, which, in turn, are short compared with the muon decay time  $\approx$   $\mu$ s.

Thus, the time for a cycle is mainly given by the average time the  $\mu$  spends as  $d\mu$  waiting to transfer to t plus the average time it then spends as  $t\mu$  waiting to form  $dt\mu$ ,

$$\tau_c \approx \tau_{d\mu} + \tau_{t\mu}, \quad (91.25)$$

or, in terms of rates,

$$\frac{1}{\lambda_c} \approx \frac{q_{1s}c_d}{\lambda_{dt}c_t} + \frac{1}{\lambda_{dt\mu}c_d}, \quad (91.26)$$

where  $c_d$  and  $c_t$  are the fractions of deuterium and tritium ( $c_d + c_t = 1$ ),  $\lambda_{dt}$  is the d-to-t transfer rate in the 1s state,  $q_{1s}$  is the fraction of  $d\mu$  atoms reaching the 1s state (before transfer), and  $\lambda_{dt\mu}$  is the molecular formation rate. The factor  $q_{1s}$  takes into account the fact that any transfer in excited states is rapid (of necessity, since it must compete with the rapid deexcitation).

The cycle rate  $\lambda_c$  along with the sticking fraction  $\omega_s$  constitute the two basic parameters of the catalysis cycle. The average number of fusions per muon  $Y$  is given by

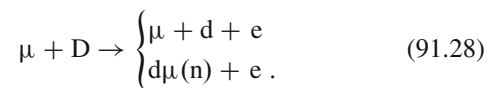
$$\frac{1}{Y} \approx \frac{\lambda_0}{\lambda_c} + \omega_s, \quad (91.27)$$

where  $\lambda_0 (\equiv 1/\tau_0)$  is the muon-decay rate. (Note: more precisely,  $W$  should appear in Eq. (91.27) in place of  $\omega_s$ ;  $W$  may include other losses, e.g., muon capture by impurities, but we will restrict the present discussion to  $\omega_s$ , which is fundamental and normally dominant.) Coincidentally, the limits imposed on the yield by the cycling rate and by sticking are similar; for  $\phi \approx 1$  and  $T \approx 300$  K,  $\lambda_c/\lambda_0 \approx 300$  and  $1/\omega_s \approx 200$  for  $dt\mu$ . More than 100 muon-catalyzed d-t fusions per muon have been observed. Similar considerations apply to the  $dd\mu$  cycle, and, by further coincidence, the two limits are similar there as well,  $\lambda_c^{dd\mu}/\lambda_0 \approx 7$  and  $1/\omega_s^{\text{eff}(dd\mu)} \approx 14$ . (Note: the effective sticking probability (per cycle) takes into account that in only 58% of the fusion reactions is a  ${}^3\text{He}$  produced that can remove the  $\mu$  by sticking. Sticking to t or p is possible but would facilitate rather than terminate the cycling.) The four experimental knobs are the temperature ( $T$ ), density ( $\phi$ ), isotopic fractions ( $c_t$ ,  $c_d$ , and  $c_p$ ), as well as the molecular fractions ( $c_{D_2}$ ,  $c_{DT}$ ,  $c_{T_2}$ ,  $\dots$ ) in the case of a target not in chemical equilibrium.

Each stage of the cycle is discussed in the following sections. The reader is referred to the reviews [97, 106–110] for details of the theoretical and experimental methods and extensive values of the relevant parameters.

### 91.4.2 Muon Atomic Capture

The  $\mu$ CF process starts with a free muon, injected into a mixture of hydrogen isotopes, being stopped to form a muonic atom. The slowing and capture occur primarily by ionization, e.g.,



In this reaction, the muon is captured into an orbital with  $n \gtrsim \sqrt{m_\mu/m_e} \approx 14$ , which has about the same size and energy as that of the displaced electron. For a review of atomic capture of negative particles, see [111].

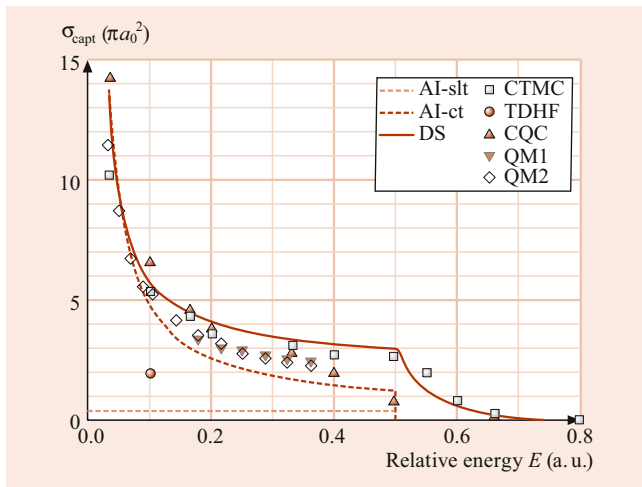


**Fig. 91.3** Comparison of different capture cross sections for  $\mu^- + \text{H}$  collisions: adiabatic ionization with straight-line trajectories (AI-slt), adiabatic ionization with curved trajectories (AI-ct), diabatic states with polarized orbital (DS), classical-trajectory Monte Carlo (CTMC), time-dependent Hartree–Fock (TDHF), classical-quantal coupling (CQC), quantum mechanical wavepacket (QM1), and Chew–Goldberger integral equation (QM2)

Early calculations were done using the Born or Coulomb–Born approximation [112]. These methods are not very accurate for  $\mu^-$  at velocities below 1 a.u., but, more importantly, their implementation treated slowing down and capture inconsistently. The upshot was prediction of capture of muons at kinetic energies of hundreds of eV, whereas it turns out that most captures actually do not occur until the muon is slowed to energies below 100 eV.

The perturbative methods failed because of the great electron charge redistribution that occurs during the capture process. Other approaches have led to progressively more accurate treatment:

1. Adiabatic ionization with straight-line trajectories (AI-slt) [113]
2. Adiabatic ionization with curved trajectories (AI-ct) [114, 115]
3. Diabatic states (DS) [116, 117]
4. Classical-trajectory Monte Carlo (CTMC) [115]
5. Time-dependent Hartree–Fock (TDHF) [118]
6. Classical-quantal coupling (CQC) [119]
7. Quantum mechanical wavepacket (QM1) [120]
8. Chew–Goldberger integral equation (QM2) [121].

Results for the capture cross sections are shown in Fig. 91.3.

The early study by *Wightman* [113] shed a great deal of light on the capture process. His method, known as adiabatic ionization (AI), followed from the observation of *Fermi* and *Teller* [122] that there exists a critical value of the dipole moment  $eR_c$ , formed by the negative muon and positive proton at distance  $R_c = 0.639 a_0$ , for binding the electron. In colli-

sions where the  $\mu^-$  approaches closer than this distance, the electron is assumed to escape adiabatically, and, if the electron carries off more energy than the muon’s initial kinetic energy, the  $\mu\mu$  atom is formed. This cross section is thus

$$\sigma_{\text{AI-slt}} = \pi R_c^2, \quad (91.29)$$

and  $\mu^-$  capture results if and only if  $E < 0.5$  a.u., the target ionization energy.

The AI-slt model has three major shortcomings: (1) it does not take into account trajectory curvature, which is caused by the Coulomb attraction of the negative muon toward the positive nucleus and can be large at the low-trajectory velocities where capture usually occurs, (2) the adiabatically escaping electron takes off no kinetic energy, and (3) ionization occurs with unit probability if the approach is closer than  $R_c$ . The first failing is easy to remedy. The cross section with curved adiabatic trajectories (AI-ct) is just [115]

$$\sigma_{\text{AI-ct}} = \frac{\pi R_c^2}{E} \left( E + \frac{1}{R_c} - 0.5 \text{ a.u.} \right), \quad (91.30)$$

as long as the collision energy  $E$  in the center-of-mass system is greater than 0.03 a.u. (0.8 eV). Hence, trajectory curvature increases the capture cross section by a factor  $1 + (1.06/E)$  (for  $E$  in a.u.), which is over a factor of 3 even at the highest collision energy (0.5 a.u.) where adiabatic capture can occur. For  $E < 0.03$  a.u., the centrifugal barrier in the effective potential,

$$V_{\text{a(eff)}}(R, b) = V_{\text{a}}(R) + \frac{b^2}{R^2} E, \quad (91.31)$$

restricts penetration and reduces the cross section below the value given by Eq. (91.30) [114].

Cures for the second and third failings are less trivial. These two assumptions were first avoided by using the diabatic-states (DS) model [116, 117]. The adiabatic electronic potential energy no longer increases once it reaches the continuum ceiling; however, in view of the  $\mu^-$  acceleration by the Coulomb attraction, the electron cloud actually does not have enough time to adjust adiabatically. In recognition of this situation, the diabatic treatment yields an electronic potential energy that crosses into the continuum at a distance larger than  $R_c$  and continues to rise smoothly. The concomitant probability of ionization is given by the ionization width, obtained from a Fermi-golden-rule-like formula. The next method applied was classical-trajectory Monte Carlo (CTMC) [115], discussed in Chap. 62. The CTMC method treats the dynamics of all particles exactly but classically. The classical approximation was later eliminated by using the time-dependent Hartree–Fock (TDHF) method discussed in Sect. 53.3 [118]. However, the improvement was open to question since it was achieved at the expense of



neglecting correlation, which turns out to be important in the present problem. This deficiency was remedied by the classical-quantal coupling (CQC) method, which makes only the seemingly well-justified approximation of treating the muon classically while retaining the quantum treatment of the electron [119]. Since then, there have been two rigorous quantum-mechanical calculations [120, 121] using time-dependent methods. These calculations have been limited to collision energies below 10 eV (0.37 a.u.). At very low energies, especially in view of the resonance behavior found [120], the time-dependent methods require quite time-consuming computations. Recently, the capture cross section was also calculated quantum mechanically by the time-independent  $R$ -matrix method, which was able to better characterize the resonances; this calculation was done only for very low energies (below 1 eV) [123]. Except for the adiabatic ionization and TDHF methods, the results of the various methods are generally in fairly good agreement, although calculations for  $E_{\text{cm}} > 0.5$  a.u. are more challenging, and the classical results have yet to be confirmed by completely quantum mechanical calculations.

Real  $\mu^-$  capture experiments (and  $\mu\text{CF}$ ) are generally done with molecules ( $\text{H}_2$ ,  $\text{DT}$ , etc.). The naive notion, once accepted, that the  $\text{H}_2$  cross section is simply twice that of  $\text{H}$  is quite unrealistic for slow ( $v \ll 1$  a.u.) collisions. The capture by hydrogen molecules, which is the first step in  $\mu\text{CF}$ , is now theoretically much better understood [124]. The molecular cross section is greatly enhanced, primarily due to the molecular vibrational degree of freedom, which enables the molecule to capture  $\mu^-$  at collision energies up to  $\approx 40$  eV in hydrogenic states with principal quantum number  $n \gtrsim 9$ , whereas atomic capture cuts off above  $\approx 14$  eV with  $n \gtrsim 14$ . There is a corresponding isotope effect in the molecule, which is absent in the atom.

### 91.4.3 Muonic Atom Deexcitation and Transfer

The muon is captured in a highly excited state but normally must reach the  $1s$  configuration of the heavier isotope (in the case of mixtures like  $D/T$ ) before the muonic molecule is formed. In the  $1s$  configuration, there are two hyperfine levels – the ground state with the nuclear and  $\mu^-$  spins antiparallel and an excited state with spins parallel. Resonant molecular formation rates in the two states can be quite different and also depend strongly on the atom's kinetic energy. Thus, there are several types of muonic atom collisions that must be taken into account: (1) elastic scattering in the ground and excited states, (2) isotopic transfer in excited states, (3) deexciting transitions (which may also occur radiatively), (4) isotopic transfer in the  $1s$  state, and (5) hyperfine transitions. Cross sections for most of these processes have been calculated. The bulk of the calcula-

tions have been done by expanding in adiabatic (or modified adiabatic) eigenfunctions, but there also exist some calculations using the coupled-rearrangement-channel, Faddeev, hyperspherical, and variational approaches ([97, 107] for references).

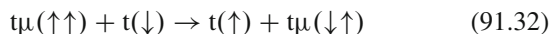
The cascade of the initially formed muonic atom, especially in mixtures, is a complicated process [125]. It constitutes a crucial part of the  $d$ - $t$   $\mu\text{CF}$  cycle in that it determines the parameter  $q_{1s}$  in Eq. (91.26). This parameter is essential to experimental analysis, but it was evident that early calculations yielded values of  $q_{1s}$  too small to be consistent with experiments. Theoretical calculations suggest the explanation is that the excited muonic atoms are not thermalized [126–128]. Epithermal atoms have three effects here: (1) the normal transfer rates are smaller, (2) the transfer is reversible down to lower principal quantum numbers  $n$  where  $E$  still exceeds the threshold for excitation of the next-higher level, and (3) excited-state [from  $(t\mu)^*$ ] resonant formation of  $(d\mu)^*$  molecules that can predissociate back to  $d\mu$  is enhanced [129]. (*Note:* the isotopic energy splittings are  $134.7/n^2$  for  $d\mu$ - $p\mu$ ,  $182.8/n^2$  for  $t\mu$ - $p\mu$ , and  $48.0/n^2$  for  $t\mu$ - $d\mu$ .) The parameter  $q_{1s}$  is determined by competition between transfer and deexcitation, which depend on the kinetic energies that result from further competition between superelastic deexcitation and thermalizing elastic collisions. It appears that the stage of the cascade most crucial for  $q_{1s}$  is  $n \approx 4$  for normal muon transfer and  $n = 2$  for the resonant sidepath.

In contrast with electrons, for muons the elastic cross sections are more difficult to calculate than the inelastic ones. The inelastic transitions occur at short range (a few  $a_\mu$ ) where the effects of electronic structure are negligible. However, electronic effects are not negligible for low-energy ( $< 1$  eV) elastic scattering where  $\lambda_{\text{dB}} \approx 1 a_0$ . They have been taken into account for ground state but not yet excited-state scattering. In doing so, it is not necessary to solve the general problem directly because of the following simplifications: (1) this energy is below the vibrational threshold, so the molecular target can be taken as a rigid rotor, and (2) the relative smallness of the muonic atoms makes the sudden approximation adequate.

If the  $1s$  state is reached without muon transfer to the heavier isotope already having occurred, the transfer takes significant time and plays an important role in determining the tritium fraction  $c_t$  that optimizes the fusion yield. All of the  $1s$  isotopic-exchange cross sections display the characteristic  $\approx 1/v$  velocity dependence at thermal energies, so that the corresponding rate  $v\sigma$  is independent of temperature.

In muon-catalyzed  $d$ - $d$  and  $d$ - $t$  fusions, the resonant molecular formation rates in different hyperfine structure (HFS) states can differ by two or more orders of magnitude at low  $T$  due to their different energy levels. The HFS also has important effects on thermalization and diffusion

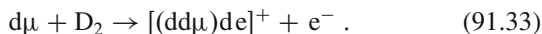
via the different elastic cross sections. Under usual  $\mu\text{CF}$  experimental conditions, the hyperfine quenching (or *spin flip*) is irreversible; the HFS splittings are 0.1820, 0.0485, and 0.2373 eV for  $p\mu$ ,  $d\mu$ , and  $t\mu$ , respectively. Theoretically, it is expected that transitions between HFS levels mainly occur in symmetric collisions since muon exchange suffices in such collisions [130]; e.g.,



(the usual terminology here is *muon exchange*, although it might seem more logical to refer to the reaction as *triton exchange* since it is the identity of the tritons that enables the reaction). As in the case of the isotopic exchange cross sections, the behavior is  $\approx 1/v$  at thermal energies, so the rates are nearly independent of temperature.

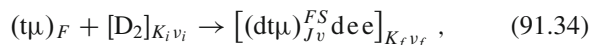
#### 91.4.4 Muonic Molecule Formation

Until the prediction by *Vesman* [131] of a resonant formation for  $dd\mu$ , it was thought that all muonic molecules were formed by an Auger process of the type



Unlike the resonant process for  $dd\mu$  and  $dt\mu$ , the nonresonant process generally depends weakly on the temperature of the target, the hyperfine state of the muonic atom, and the *spectator* atom  $X$  in the molecule  $DX$ , where  $X$  can be H, D, or T. The nonresonant rate at low (liquid hydrogen) temperature for  $dd\mu$  formation is about  $3 \times 10^4 \text{ s}^{-1}$ , and for  $dt\mu$  it is about  $6 \times 10^5 \text{ s}^{-1}$ . These rates are competitive with the resonant rates at low  $T$  for  $d\mu(\uparrow\downarrow) + D_2$  and  $t\mu(\uparrow\uparrow) + D_2$ , but are two and three orders of magnitude smaller than the resonant rates for  $d\mu(\uparrow\uparrow) + D_2$  and  $t\mu(\uparrow\downarrow) + D_2$ , respectively. The  $(\uparrow\downarrow)$  state is the ground state; thus HFS quenching plays an important role in low-temperature experiments, especially for  $dd\mu$ . At room temperature, resonant formation is dominant for both the ground and excited hyperfine states of  $d\mu$  and  $t\mu$ .

In the *Vesman* mechanism, the binding energy of the muonic molecule goes into rovibrational excitation of the electronic host molecule instead of into ionization of a molecular electron. The process is resonant since the collision energy must be tuned to match the energy of the final discrete state. For the compound molecule formed, two sets of rovibrational quantum numbers are needed, e.g.,



where  $(K_i, v_i)$  and  $(K_f, v_f)$  are the initial and final rovibrational quantum numbers of the electronic molecule,  $(J, v)$

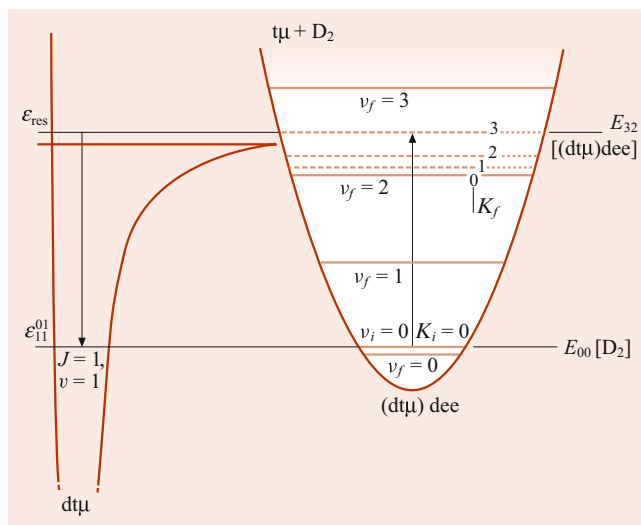


**Fig. 91.4** Energy levels for the resonant reaction  $t\mu + [D_2]_{K_i=0, v_i=0} \rightarrow [(dt\mu)_{J=1, v=1}^{F=0, S=1} \text{dee}]_{K_f v_f}$ . The rovibrational quantum numbers are designated by  $(J, v)$  for the muonic molecule and  $(K, v)$  for the electronic molecules

are the quantum numbers of the muonic molecule,  $F$  is the spin of the muonic atom, and  $S$  is the total spin of the muonic molecule. The energetics of this process is shown in Fig. 91.4.

The resonant condition is achieved at the collision energy

$$\epsilon_{\text{res}}(t\mu + D_2) = \epsilon_{11}^{FS} [dt\mu] + E_{K_f v_f} [(dt\mu)\text{dee}] - E_{K_i 0} [D_2] , \quad (91.35)$$

where it is explicitly recognized that  $(J, v) = (1, 1)$  is the only muonic level that can satisfy the resonant energy condition and that only  $v_i = 0$  is populated at ordinary temperatures. Accurate calculations require values of  $\epsilon_{\text{res}}$  to within about 0.1 meV. The rovibrational energies  $E_{K v}$  of the electronic molecule, as well as the Coulomb contributions to the binding energy of the muonic molecule,  $\epsilon_{11}^{FS}$ , are now known to this high accuracy. However,  $\epsilon_{11}^{FS}$  is subject to corrections due to relativity, vacuum polarization, nuclear charge distributions and polarizabilities, the hyperfine interaction, and the finite size and shape of the muonic molecule in the complex. The present overall accuracy is  $\approx 1$  meV. Some of the resulting values of  $\epsilon_{\text{res}}$  are given in Table 91.1. The calculated cross section for reaction Eq. (91.34) is sharply peaked at  $E_{\text{res}}$  but must be averaged over a kinetic energy distribution (e.g., Maxwellian) to obtain the observable rate. Still, the rate will display a characteristic resonant dependence on  $T$ .

Because the  $E_{\text{res}}$  are different for each target molecule ( $D_2$ ,  $DT$ ,  $T_2$ ,  $\dots$ ), the effective molecular formation rate in a mixture depends on the molecular composition in addition to the isotopic fractions ( $c_d$ ,  $c_t$ ,  $\dots$ ) if the target is not in chemical equilibrium.

**Table 91.1** Resonant (quasiresonant if negative) collision energies  $\epsilon_{\text{res}}$  (in meV) calculated using Eq. (91.35)<sup>a</sup>

$d\mu + D_2$		$t\mu + D_2$		$t\mu + DT$	
$[(dd\mu)_{11}dee]_{v_f=7}$		$[(dt\mu)_{11}dee]_{v_f=2}$		$[(dt\mu)_{11}tee]_{v_f=3}$	
$F, S, K_i, K_f$	$\epsilon_{\text{res}}$	$F, S, K_i, K_f$	$\epsilon_{\text{res}}$	$F, S, K_i, K_f$	$\epsilon_{\text{res}}$
$\frac{1}{2}, \frac{1}{2}, 0, 1$	52.7	0, 1, 0, 1	-14.0	0, 1, 0, 1	277.1
$\frac{1}{2}, \frac{3}{2}, 0, 1$	76.9	0, 1, 0, 2	-4.3	1, 0, 0, 1	223.5
$\frac{3}{2}, \frac{1}{2}, 0, 1$	4.2	0, 1, 0, 3	10.3	1, 1, 0, 1	226.9
$\frac{3}{2}, \frac{3}{2}, 0, 1$	28.4	0, 1, 1, 2	-11.7	1, 2, 0, 1	233.3
$\frac{1}{2}, \frac{1}{2}, 1, 0$	40.9	0, 1, 1, 3	2.9		
$\frac{1}{2}, \frac{3}{2}, 1, 0$	65.1				
$\frac{1}{2}, \frac{1}{2}, 1, 2$	54.1				
$\frac{1}{2}, \frac{3}{2}, 1, 2$	78.3				

<sup>a</sup> Note:  $kT = 1$  meV for  $T = 11.6$  K

The rate of resonant molecular formation is given by

$$\lambda^{mf}(T) = N \sum_f \int \left\{ d\epsilon 2\pi |\langle i | \hat{V} | f \rangle|^2 \times f(\epsilon, T) I(\epsilon - \epsilon_{if}, T) \right\}, \quad (91.36)$$

where  $N$  is the target density,  $f(\epsilon, T)$  is the collisional energy distribution,  $\epsilon_{if}$  is the energy of the unperturbed resonance,  $I(\Delta\epsilon, T)$  is the intensity at energy  $\Delta\epsilon$  relative to the unperturbed energy, and  $\langle i | \hat{V} | f \rangle$  is the transition matrix element, with  $\hat{V}$  the Coulomb perturbation operator in the *post* form of the rearrangement-collision Hamiltonian using the  $dt\mu$  bound state as the zeroth-order Hamiltonian;  $\hat{V}$  can be expressed as a multipolar expansion beginning with

$$\hat{V} = e^2 \mathbf{d} \cdot \mathbf{E} + \dots, \quad (91.37)$$

where  $\mathbf{d}$  is the dipole operator of the  $dt\mu$  (or  $dd\mu$ ) system, and  $\mathbf{E}$  is the electric field at the  $dt\mu$  (or  $dd\mu$ ) center of mass due to the *spectator* nucleus and electrons [132]. A calculation has been done including the quadrupole term [133], but the dipole term is dominant. In the dipole approximation [134] conservation of angular momentum requires [135]

$$\mathbf{L} + \mathbf{K}_i = \mathbf{J} + \mathbf{K}_f, \quad (91.38)$$

where  $\mathbf{L}$  is the orbital angular momentum of relative motion for  $t\mu + D_2$  in reaction Eq. (91.34). At low  $T$ ,  $L = 0$  is predominant, so that  $K_f = K_i \pm 1$ . This is simply the case for  $d\mu + D_2 \rightarrow (dd\mu)dee$ , where the most probable transition is  $(K, v) = (0, 0) \rightarrow (1, 7)$ . For  $dt\mu$ , the vibrational state of the electronic molecule changes by only  $\Delta v_i = 2$  or 3 instead of 7, so the matrix element of Eq. (91.37) and the resulting rate are considerably larger than for  $dd\mu$ . However, it can be seen in Fig. 91.4 that if  $D_2$  is in its ground state ( $K_i = 0$ ), the first level energetically accessible for  $(dt\mu)dee$  has  $K_f = 3$ . If, as proves to be adequate in the case of  $dd\mu$ , the intensity

distribution  $I$  is taken to be a  $\delta$  function, the lower levels are eliminated from Eq. (91.36). There are two possible solutions to this problem, whose relative importance has not been fully determined: (1) the less likely  $L > 0$  collisions contribute, or (2) the levels with smaller  $K_f$  play a role even though they lie *below threshold*.

The latter case is termed *quasi resonant*. Theoretically, the levels below threshold can contribute (1) directly if they are broadened so that they extend to positive energy [136–138], or (2) indirectly if configurations with different  $K_f$  are mixed [139]. Broadening can occur either inhomogeneously due to the finite lifetime (mainly with respect to Auger emission of an electron in the complex) or homogeneously due to collisions with neighboring molecules. Interactions with neighboring molecules can also mix the different  $K_f$  states, so the  $K_f = 3$  state may *borrow* some intensity from the lower  $K_f$  states. Three-body molecular formation facilitated by neighboring molecules leads to a density dependence of the formation rate (normalized to LHD) that has been observed in experiments.

There have been a number of measurements of the  $dd\mu$  molecular-formation rate for various target densities and temperatures. However, the epithermal effect due to nonthermalized  $d\mu$  may be significant and makes a full understanding of the temperature dependence a little difficult, especially at low temperatures. Further measurements have been carried out [140, 141] by controlling the initial molecular state ( $K_i$ ) with the use of ortho- $D_2$  ( $K_i = 0, 2, \dots$ ) and normal or even para-rich ( $K_i = 1, 3, \dots$ )  $D_2$ . These measurements have clarified the dependence on the molecular state and the density. The resonant formation rate with ortho- $D_2$  was found to be much larger than with normal  $D_2$  in the gas around 35 K, while its rate is reduced by nearly half at liquid density, even smaller than for normal- $D_2$ . This finding indicates that the resonance with ortho- $D_2$  must be very close to the threshold, and that the target density could be affecting its shift or broadening.

The resonant  $dd\mu$  formation has now been observed directly [142]. Previously, the experimental evidence for this

mechanism was derived from the magnitude and the temperature dependence of the  $\mu\text{CF}$  cycling rate [143]. The new experiment, at TRIUMF, obtained the energy-dependent molecular-formation rate by measuring the time of flight between a cryogenic layer where the  $\text{t}\mu$  atom was formed and a second cryogenic layer where the  $\text{dt}\mu$  molecule was formed, and fusion occurred.

### 91.4.5 Fusion

Usually, the nuclear fusion rate in muonic molecules is calculated by a separable method; i.e., the united-atom limit of the molecular wave function is determined ignoring nuclear forces and then simply multiplied by a single number extracted from nuclear scattering experiments [144]. Fusion of d-t is strongly dominated by the  $I^\pi = (3/2)^+$  resonance of  $^5\text{He}$ . For  $\text{dt}\mu$ , we have

$$\lambda_{\text{dt}\mu}^f = A \lim_{r_{\text{dt}} \rightarrow 0} \int |\psi_{\text{dt}\mu}|^2 d^3 r_\mu, \quad (91.39)$$

where  $A$  is simply related to the low-energy limit of the astrophysical  $S$  factor by

$$A = \frac{\hbar}{\pi e^2 M_r} \lim_{E \rightarrow 0} S(E), \quad (91.40)$$

where  $M_r$  is the reduced mass of the nuclei;  $S(E)$  is usually obtained by fitting the d + t fusion cross section observed in beam experiments to the form of Eq. (91.18).

The above formulation has yielded fusion rates in good agreement with another formulation – more accurate in principle – where a complex molecular wave function and energy are obtained directly incorporating the nuclear forces. In the latter approach,

$$\lambda_{\text{dt}\mu}^f = -2 \text{Im}(E_{\text{dt}\mu})/\hbar, \quad (91.41)$$

where  $E_{\text{dt}\mu}$  is the complex eigenvalue (the imaginary part is  $-\Gamma/2$ , where  $\Gamma$  is the width). The nuclear effect in this formulation is taken into account by two different techniques: (1) using a complex optical potential [145, 146] (Sect. 51.2), and (2) using the nuclear  $R$ -matrix as an interior boundary condition [147–149] (Sect. 49.1.4). In the optical potential method, a short-range complex potential, determined by fitting experimental nuclear scattering data, is added to the three-body Coulomb potential; the real part describes elastic scattering and the imaginary (absorptive) part describes the fusion reaction. Then the eigenvalue problem is solved over all space with a regular boundary condition at the origin. In the  $R$ -matrix method, the same nuclear scattering data are used to determine a complex boundary condition at a distance characteristic of the nuclear forces, say  $r_{\text{dt}} = a_{\text{dt}}$  where

$a_{\text{dt}} \approx 5$  fm. The muonic eigenvalue problem is then formulated with the boundary condition at  $r_{\text{dt}} = a_{\text{dt}}$  and solved over the space excluding  $r_{\text{dt}} < a_{\text{dt}}$ . The two methods can be used with similar basis sets to expand the wave function, which can also be used to calculate the sticking probability (Sect. 91.4.6).

The relation of other  $\mu\text{CF}$  cross sections to normal beam experiments is somewhat more complicated. In the cases of  $\text{dd}\mu$  and  $\text{tt}\mu$ , the fusion may occur in  $J = 1$  states, since the  $J = 1$  to  $J = 0$  transition is forbidden in molecules with identical nuclei. In this case, the relevant information from beam experiments resides in the p-wave anisotropy, which is relatively small at low energies, where  $\sigma$  is dominated by the s wave. It is then necessary to carry out the analysis in terms of the partial-wave transition amplitudes rather than the fit of the integrated  $\sigma$  via the  $S$  factor [150].

Fusions in  $\text{pd}\mu$  and  $\text{pt}\mu$  present a different complication [144]. There is a significant  $E0$  contribution from muon conversion in addition to the  $M1$   $\gamma$ -ray contribution seen in p + d and p + t beam experiments (for a discussion of multipole moments: Sect. 13.1). The  $E0$  contribution cannot be expressed through cross sections observed in the beam experiments but has been determined using the bound-state nuclear wave functions of  $^3\text{He}$  (or  $^4\text{He}$ ) and scattering wave functions of p + d (or p + t). For  $\text{pd}\mu$ , there is the additional complication that two different p – d spin states contribute significantly. For  $\text{pt}\mu$ , theory [144] predicts that the probability of the fusion energy going into a  $e^+e^-$  pair is competitive with that of muon conversion, although the former has not yet been observed.

### 91.4.6 Sticking and Stripping

The fundamental mechanism of muon loss from the catalysis cycle, other than by particle decay, is via sticking to a helium nucleus,  $^4\text{He}$  or  $^3\text{He}$ , produced in the fusion reaction. Especially in the case of  $\text{dt}\mu$ , where the charged particle is fast and the sticking probability is already small, subsequent collisions may strip the muon. Thus, the sticking probability is determined by two steps

$$\begin{array}{c} \text{dt}\mu \longrightarrow \begin{array}{l} 1 - \omega_s^0 \nearrow \alpha + \mu + n \\ \omega_s^0 \searrow \alpha\mu (3.5 \text{ MeV}) + n \\ \phantom{\omega_s^0 \searrow} \downarrow \begin{array}{l} R \nearrow \alpha + \mu \\ \phantom{R \nearrow} \searrow \alpha\mu (\text{thermal}) \end{array} \\ \phantom{\omega_s^0 \searrow} \phantom{\downarrow} 1 - R \end{array} \end{array} \quad (91.42)$$

The initial sticking probability  $\omega_s^0$  depends only on intramolecular dynamics, but the stripping conditional probability depends on collisions. (Note that  $\omega_s^0$  is not the sticking

in the zero-density limit since  $R$  is still finite in this limit.) The net sticking is then

$$\omega_s = \omega_s^0(1 - R). \quad (91.43)$$

Since the nuclear reaction is very rapid compared with the atomic and molecular dynamics, the probability of sticking in a given state  $\nu$  is given adequately by the sudden approximation,

$$P_\nu = |\langle \psi_\nu^{(f)} | \psi^{(i)} \rangle|^2, \quad (91.44)$$

where the initial wave function  $\psi^{(i)}$  is the normalized molecular wave function in the limit  $r_{\text{dt}} \rightarrow 0$ , and the final wave function  $\psi_\nu^{(f)}$  is given by

$$\psi_\nu^{(f)} = \phi_{n\ell m}(\mathbf{r}) e^{i\mathbf{q}\cdot\mathbf{r}}, \quad (91.45)$$

in which  $\phi_{n\ell m}$  is an atomic wave function of  $({}^4\text{He}\mu)^+$ , and the plane wave with momentum  $\mathbf{q}$  represents its motion with respect to the initial molecule (recoil determined by conservation of energy and momentum). The total sticking is then

$$\omega_s^0 = \sum_\nu P_\nu. \quad (91.46)$$

The  $({}^4\text{He}\mu)^+$  wave function is known analytically since it is hydrogenic. Most of the labor goes into determination of the muonic molecule wave function. In the Born–Oppenheimer approximation this is simply  $({}^5\text{He}\mu)^+$  and results in  $(\omega_s^0)_{\text{BO}} = 1.20\%$  for  $\text{dt}\mu$  [151]. More accurate nonadiabatic calculations show that the muonic motion lags behind that of the nuclei and reduces  $\omega_s^0$  to 0.886% [152, 153]. After inclusion of nuclear effects, the best current theoretical value of  $\omega_s^0$  is 0.912% [149, 154].

Since the ground-state  $(\text{He}\mu)^+$  ion is bound by 11 keV, it takes a quite energetic collision to strip off the muon. The reactivation fraction  $R$  is determined basically by competition between collisional processes that slow down the muonic ion and those that lead to stripping. Calculation of  $R$  requires a full kinetic treatment of the fast  $(\text{He}\mu)^+$  ion, starting with its distribution among various states (1s, 2s, 2p,  $\dots$ ,  $n \approx 10$ ). The most important processes are stopping power (due mainly to ionization of the medium) and muon ionization or transfer in collisions of the  $(\text{He}\mu)^+$  ion with an isotope of H, but inelastic (excitation and deexcitation), Auger deexcitation, and  $\ell$ -changing collisions, as well as radiative deexcitation are also involved. The initial sticking occurs mostly in the 1s state (77% of the  $\alpha\mu$ 's from  $\text{dt}\mu$  fusion), but the excited states have larger ionization cross sections. Most of the muons stripped from  $\alpha\mu$  originally stuck in the 1s state, but a significant number is promoted to excited states before being ionized (so-called *ladder ionization*). The

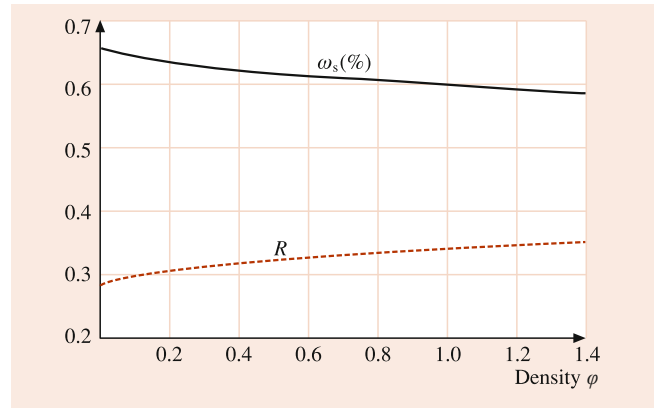


**Fig. 91.5** Theoretical sticking fraction (solid curve) and reactivation probability (dashed curve) for d-t  $\mu\text{CF}$

metastable 2s state is significant for its role in prolonging the excited-state populations. The resulting values of  $R$  and  $\omega_s$  are shown as a function of density in Fig. 91.5.

Most experiments on d-t  $\mu\text{CF}$  have been done with neutron detection [155–157], where  $\lambda_c$  and the muon loss probability per cycle  $W$  can be deduced from the time structure of the neutron emissions. The analysis is indirect and requires a theoretical model. What is actually measured is the product  $W\phi\lambda_c$ ; the extraction of  $\omega_s$  requires corrections for other loss mechanisms and separate determination of  $\lambda_c$ . Thus, it is desirable to have other experimental diagnostics. Two types of corroborating experiments detect either X-rays from the  $\alpha\mu$  formed by sticking or detect the species  $(\alpha)^{2+}$  and  $(\alpha\mu)^+$  by the different effects of their double and single electrical charges.

The theoretical sticking is compared in Table 91.2 with that from all three types of experiments. For a more meaningful comparison of measurements at different densities  $\phi$ , the theoretical  $R$  has been used to convert all values to  $\omega_s^0$ . The theoretical values are slightly, but significantly, higher than the observations. This discrepancy has not yet been resolved.

One suggested explanation for the lower-than-predicted value of  $\omega_s$  may be that a significant fraction of the fusions might occur in muonically excited bound or resonant states for which the initial sticking is lower than in the ground state [158].

A 2003 experiment systematically studied muon-catalyzed fusion in solid deuterium and tritium mixtures as a function of temperature and tritium concentration [159]. An unexpected decrease in the muon cycling rate ( $\lambda_c$ ) and an increase in the muon loss ( $W$ ) were observed. The former is likely due to the freezing out of phonons contributing to the resonance energy. The latter is especially intriguing. It is inconceivable that  $\omega_s^0$  for fusion in a given state of  $\text{dt}\mu$  could depend on temperature, but this observation could imply either an unexpected effect of temperature on the muonic state in which fusion occurs or an unpredicted temperature

**Table 91.2** Comparison of sticking values<sup>a</sup>

Source	$\phi$	$\omega_s$ (%)	$\omega_s^0$ (%)
Theory			
[149, 154]	1.2	0.59	0.91
Neutron experiments			
LANL [165]	$\approx 1$	$0.43 \pm 0.05 \pm 0.06$	0.66
PSI [166]	$\approx 1$	$0.48 \pm 0.02 \pm 0.04$	0.74
KEK [167]	1.2	$0.51 \pm 0.004$	0.78
RAL [168]	1.24	$0.532 \pm 0.030$	0.82
RAL [168]	1.45	$0.515 \pm 0.030$	0.79
X-ray experiments			
PSI [169]	1.2	$0.39 \pm 0.10$	0.60
KEK [167]	1.2	$0.34 \pm 0.13$	0.52
$\alpha/\alpha\mu$ experiments			
RAL [170]	0.001	–	$0.80 \pm 0.15 \pm 0.12$
PSI [171]	0.17	$0.56 \pm 0.04$	0.80

<sup>a</sup> Experimental values of  $\omega_s^0$  without error bars were obtained assuming the theoretical stripping [172, 173].

In cases of two error estimates, the first is statistical and the second is systematic.

The extraction of  $\omega_s^0$  from the X-ray experiments requires theoretical scaling

dependence of the thermalization kinetics (e.g., due to ion channeling). It should be noted that the experimental analysis does not reject the possibility of some correlation between the extracted values of  $\lambda_c$  and  $W$  [158].

### 91.4.7 Prospectus

Muon-catalyzed d-d fusion in D<sub>2</sub> and HD gases has now been investigated in a wide temperature range, with all the main observables in the reaction chain accurately measured [101, 160]. The energy of the loosely bound dd $\mu$  was extracted with high precision [101], and it is in impressive agreement with the latest theoretical results. The experimental knowledge of parameters for p-t  $\mu$ CF [105] and t-t  $\mu$ CF [103] have also been advanced.

The d-t  $\mu$ CF is now fairly well understood [102], but investigations under broader conditions of temperature and density are still desirable; in particular, three-body effects on molecular formation at high densities, the excited-state cross sections and kinetics that go into the determination of the cascade factor  $q_{1s}$ , and the remaining discrepancy in the sticking factor  $\omega_s$ , which might have a theoretical or experimental resolution. Experimentally it is of interest to push on to higher temperatures and densities to see whether more surprises lurk there. There have been a few schemes proposed to enhance stripping of stuck muons artificially, but none has been subjected to experiments yet.

The currently observed yield of about 150 d-t fusions (releasing 17.6 MeV each) per muon produces an energy return 25 times the rest-mass energy of the muon but is only about

one-third of that required for breakeven in a pure-fusion reactor. This conclusion is based on the estimated energy cost of producing a muon,  $\approx 8$  GeV [161, 162]. Other possible practical uses of  $\mu$ CF include a hybrid (fusion–fission) reactor [161, 162] or an intense 14 MeV neutron source [163, 164].

Apart from such technological applications, the study of  $\mu$ CF is fruitful for a number of reasons, including (1) bridging the gap between atomic and nuclear physics, (2) enabling nuclear reactions *including p-waves* at room temperature, (3) allowing precise studies under unusual physical conditions, (4) observing a compound electronic-muonic molecular environment, and (5) exhibiting phenomena spanning nine orders of magnitude in distance and energy. The experimental possibilities are far from exhausted even though the holy grail of pure fusion energy now appears just beyond reach.

**Acknowledgement** J.D.M. is grateful to the Institute for Nuclear Theory of the University of Washington for making it possible for him to spend a productive semester there in the spring of 1993. This work has also been supported by National Science Foundation grant PHY-9215442.

## References

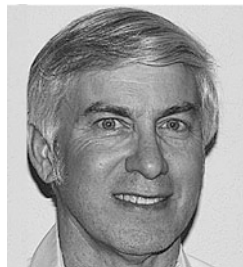
- Coester, F.: Nucl. Phys. **7**, 421 (1958)
- Coester, F., Kümmel, H.: Nucl. Phys. **17**, 477 (1960)
- Kümmel, H.: Nucl. Phys. **22**, 177 (1969)
- Cizek, J.: J. Chem. Phys. **45**, 4256 (1966)
- Cizek, J.: Adv. Chem. Phys. **14**, 35 (1969)
- Paldus, J., Cizek, J., Shavitt, I.: Phys. Rev. A **5**, 50 (1972)
- Jensen, A.S., Riisager, K., Fedorov, D.V., Garrido, E.: Rev. Mod. Phys. **76**, 215 (2004)
- Lamb, W.E., Retherford, R.C.: Phys. Rev. **72**, 241 (1950)
- Lamb, W.E., Retherford, R.C.: Phys. Rev. **79**, 549 (1950)
- Lamb, W.E., Retherford, R.C.: Phys. Rev. **81**, 222 (1951)
- Lamb, W.E., Retherford, R.C.: Phys. Rev. **86**, 1014 (1952)
- Houston, W.V., Hsieh, Y.M.: Phys. Rev. **45**, 263 (1934)
- Houston, W.V.: Phys. Rev. **51**, 446 (1937)
- Williams, R.C.: Phys. Rev. **54**, 558 (1938)
- Pasternack, S.: Phys. Rev. **54**, 1113 (1938)
- Bezginov, N., Valdez, T., Horbatsch, M., Marsman, A., Vutha, A.C., Hessels, E.A.: Science **365**, 1007 (2019)
- Pohl, R., et al.: Nature **466**, 213 (2010)
- Antognini, A., et al.: Science **339**, 417 (2013)
- Kemble, E.C., Present, R.D.: Phys. Rev. **44**, 1031 (1933)
- Karplus, R., Klein, A., Schwinger, J.: Phys. Rev. **86**, 301 (1951)
- Lamb, W.E.: Phys. Rev. **85**, 276 (1952)
- Salpeter, E.E.: Phys. Rev. **89**, 95 (1953)
- Zemach, A.C.: Phys. Rev. **104**, 1771 (1956)
- Flügge, S.: Practical Quantum Mechanics vol. I. Springer, New York, pp 191–192 (1971)
- Drake, G.W.F., Yan, Z.-C.: Phys. Rev. A **46**, 2378 (1992)
- Shiner, D., Dixon, R., Vedantham, V.: Phys. Rev. Lett. **74**, 3553 (1995)
- Riis, E., Sinclair, A.G., Poulsen, O., Drake, G.W.F., Rowley, W.R.C., Levick, A.P.: Phys. Rev. A **49**, 207 (1994)
- Pachucki, K., Weitz, K.M., Hänsch, T.W.: Phys. Rev. A **49**, 2255 (1994)
- Huber, A., Udem, T., Gross, B., Reichert, J., Kourogi, M., Pachucki, K., Weitz, M., Hänsch, T.W.: Phys. Rev. Lett. **80**, 468 (1998)

30. Wang, L.-B., Mueller, P., Bailey, K., Drake, G.W.F., Greene, J.P., Henderson, D., Holt, R.J., Janssens, R.V.F., Jiang, C.L., Lu, Z.-T., O'Connor, T.P., Pardo, R.C., Paul, M., Rehm, K.E., Schiffer, J.P., Tang, X.D.: *Phys. Rev. Lett.* **93**, 142501 (2004)
31. Ewald, G., Nörtershäuser, W., Dax, A., Göte, S., Kirchner, R., Kluge, H.-J., Kühl, T., Sanchez, R., Wojtaszek, A., Bushaw, B.A., Drake, G.W.F., Yan, Z.-C., Zimmermann, C.: *Phys. Rev. Lett.* **93**, 113002 (2004)
32. Schawlow, A.L., Townes, C.H.: *Phys. Rev.* **100**, 1273 (1955)
33. Bodmer, A.R.: *Proc. Phys. Soc. A* **66**, 1041 (1953)
34. Mohr, P.J.: *At. Data Nucl. Data Tables* **33**, 456 (1983)
35. Friar, J.L.: *Ann. Phys.* **122**, 151 (1979)
36. Johnson, W.R., Soff, G.: *At. Data Nucl. Data Tables* **33**, 407 (1985)
37. de Jager, C.W., de Vries, H., de Vries, C.: *At. Data Nucl. Data Tables* **14**, 479 (1974)
38. Raghaven, P.: *At. Data Nucl. Data Tables* **42**, 189 (1989)
39. Wapstra, A.H., Audi, G.: *Nucl. Phys. A* **432**, 1 (1985)
40. Seely, J.F., Ekberg, J.O., Brown, C.M., Feldman, U., Behring, W.E., Reader, J., Richardson, M.C.: *Phys. Rev. Lett.* **57**, 2924 (1986)
41. Cowan, T.E., Bennett, C.L., Dietrich, D.D., Bixler, J.V., Hailey, C.J., Henderson, J.R., Knapp, D.A., Levine, M.A., Marrs, R.E., Schneider, M.B.: *Phys. Rev. Lett.* **66**, 1150 (1991)
42. Schewpe, J., Belkacem, A., Blumenfeld, L., Claytor, N., Feinberg, B., Gould, H., Kostroune, V.E., Levy, L., Misawa, S., Mowat, J.R., Prior, M.H.: *Phys. Rev. Lett.* **66**, 1434 (1991)
43. Blundell, S.A., Snyderman, N.J.: *Phys. Rev. A* **44**, R1427 (1991)
44. Blundell, S.A.: *Phys. Rev. A* **46**, 3762 (1992)
45. Cheng, K.T., Johnson, W.R., Sapirstein, J.: *Phys. Rev. A* **47**, 1817 (1993)
46. Bahcall, J.N.: *Phys. Rev.* **124**, 495 (1961)
47. Clayton, D.D.: *Astrophys. J.* **139**, 637 (1964)
48. Woosley, S.E., Fowler, W.A.: *Astrophys. J.* **233**, 411 (1979)
49. Williams, R.D., Fowler, W.A., Koonin, S.E.: *Astrophys. J.* **281**, 363 (1984)
50. Chen, Z., Rosenberg, L., Spruch, L.: *Phys. Rev. A* **35**, 1981 (1987)
51. Chen, Z., Rosenberg, L., Spruch, L.: *Adv. At. Mol. Opt. Phys.* **26**, 297 (1989)
52. Chen, Z., Spruch, L.: *AIP Conference Proceedings # 189, Relativistic, Quantum Electrodynamics, and Weak Interaction Effects in Atoms*. AIP, New York, pp 460–478 (1989)
53. Lubimov, V.A., Novikov, E.G., Nozik, V.Z., Tretyakov, E.F., Kozik, V.S.: *Phys. Lett. B* **94**, 266 (1980)
54. Boris, S., Golutvin, A., Laptin, L., Lubimov, V., Nagovizin, V., Nozik, V., Novikov, E., Soloshenko, V., Tihomirov, I., Tretjakov, E., Myasoedov, N.: *Phys. Rev. Lett.* **58**, 2019 (1987)
55. Boris, S.D., Golutvin, A.I., Laptin, L.P., Lyubimov, V.A., Myasoedov, N.F., Nagovitsyn, V.V., Nozik, V.Z., Novikov, E.G., Soloshchenko, V.A., Tikhomirov, I.N., Tretyakov, E.F.: *Pis'ma Zh. Eksp. Teor. Fiz.* **45**, 267 (1987). *Sov. Phys. JETP Lett.* **45**, 333 (1987)
56. Bergkvist, K.-E.: *Phys. Scr.* **4**, 23 (1971)
57. Bergkvist, K.-E.: *Nucl. Phys. B* **39**(317), 371 (1972)
58. Martin, R.L., Cohen, J.S.: *Phys. Lett. A* **110**, 95 (1985)
59. Kolos, W., Jeziorski, B., Szalewicz, K., Monkhorst, H.J.: *Phys. Rev. A* **31**, 551 (1985)
60. Fackler, O., Jeziorski, B., Kolos, W., Monkhorst, H.J., Szalewicz, K.: *Phys. Rev. Lett.* **55**, 1388 (1985)
61. Jeziorski, B., Kolos, W., Szalewicz, K., Fackler, O., Monkhorst, H.J.: *Phys. Rev. A* **32**, 2573 (1985)
62. Szalewicz, K., Fackler, O., Jeziorski, B., Kolos, W., Monkhorst, H.J.: *Phys. Rev. A* **35**, 965 (1987)
63. Kolos, W., Jeziorski, B., Rychlewski, J., Szalewicz, K., Monkhorst, H.J., Fackler, O.: *Phys. Rev. A* **37**, 2297 (1988)
64. Fritschi, M., Holzschuh, E., Kundig, W., Petersen, J.W., Pixley, R.E., Stussi, H.: *Phys. Lett. B* **173**, 485 (1986)
65. Wilkerson, J.F., Bowles, T.J., Browne, J.C., Maley, M.P., Robertson, R.G.H., Cohen, J.S., Martin, R.L., Knapp, D.A., Helffrich, J.A.: *Phys. Rev. Lett.* **58**, 2023 (1987)
66. Robertson, R.G.H., et al.: *Phys. Rev. Lett.* **67**, 957 (1991)
67. Holzschuh, E., Fritschi, M., Kündig, W.: *Phys. Lett. B* **287**, 381 (1992)
68. Weinheimer, C., Przyrembel, M., Backe, H., Barth, H., Bonn, J., Degen, B., Edling, T., Fischer, H., Fleischmann, L., Gross, J.U., Haid, R., Hermann, A., Kube, G., Leiderer, P., Loeken, T., Molz, A., Moore, R.B., Osipowicz, A., Otten, E.W., Picard, A., Schrader, M., Steininger, M.: *Phys. Lett. B* **300**, 210 (1993)
69. Fukuda, Y., et al.: *Phys. Rev. Lett.* **81**, 1562 (1998)
70. Weinheimer, C., Degen, B., Bleile, A., Bonn, J., Bornschein, L., Kazachenko, O., Kovalik, A., Otten, E.W.: *Phys. Lett. B* **460**, 219 (1999)
71. Bonn, J., Bornschein, B., Bornschein, L., Fickinger, L., Flatt, B., Kazachenko, O., Kovalik, A., Kraus, C., Otten, E.W., Schall, J.P., Ulrich, H., Weinheimer, C.: *Nucl. Phys. B* **91**, 273 (2001)
72. Hannestad, S.: *Phys. Rev. D* **66**, 125011 (2002)
73. Robertson, R.G.H.: *Nucl. Part. Phys. Proc.* **265/266**, 7–12 (2015). arXiv:1502.00144. NOW14, Neutrino Oscillation Workshop, Conca Specchiulla (Otranto, Lecce, Italy) Sept. 7–14, 2014
74. Assenbaum, H.J., Langanke, K., Rolfs, C.: *Z. Phys. A* **327**, 461 (1987)
75. Engstler, S., Krauss, A., Neldner, K., Rolfs, C., Schröder, U., Langanke, K.: *Phys. Lett. B* **202**, 179 (1988)
76. der Schr, U., Engstler, S., Krauss, A., Neldner, K., Rolfs, C., Somorjai, E., Langanke, K.: *Nucl. Instrum. Methods B* **40/41**, 466 (1989)
77. Engstler, S., Raimann, G., Angulo, C., Greife, U., Rolfs, C., Schröder, U., Somorjai, E., Kirch, B., Langanke, K.: *Phys. Lett. B* **279**, 20 (1992)
78. Engstler, S., Raimann, G., Angulo, C., Greife, U., Rolfs, C., Schröder, U., Somorjai, E., Kirch, B., Langanke, K.: *Z. Phys. A* **342**, 471 (1992)
79. Blüge, G., Langanke, K., Reusch, H.G., Rolfs, C.: *Z. Phys. A* **333**, 219 (1989)
80. Langanke, K., Lukas, D.: *Ann. Phys. (Leipzig)* **1**, 332 (1992)
81. Langanke, K.: *Adv. Nucl. Phys.* **21**, 179 (1994)
82. Shoppa, T.D., Koonin, S.E., Langanke, K., Seki, R.: *Phys. Rev. C* **48**, 837 (1993)
83. Shoppa, T.D., Jeng, M., Koonin, S.E., Langanke, K., Seki, D.: *Nucl. Phys. A* **605**, 387 (1996)
84. Bahcall, J.N., Chen, X., Kamionkowski, M.: *Phys. Rev. C* **57**, 2756 (1998)
85. Strieder, F., Rolfs, C., Spitaleri, C., Corvisiero, P.: *Naturwissenschaften* **88**, 461 (2001)
86. Zavatarelli, S., Corvisiero, P., Costantini, H., Moroni, P.G.P., Prati, P., Bonetti, R., Guglielmetti, A., Broggin, C., Campajola, L., Formicola, A., Gialanella, L., Imbriani, G., Ordine, A., Roca, V., Romano, M., D'Onofrio, A., Terrasi, F., Gervino, G., Gustavino, C., Junker, M., Rogalla, D., Rolfs, C., Schumann, F., Strieder, F., Trautvetter, H.P.: *Nucl. Phys. A* **688**, 514 (2001)
87. Aliotta, M., Raiola, E., Gyurky, G., Formicola, A., Bonetti, R., Broggin, C., Campajola, L., Corvisiero, P., Costantini, H., D'Onofrio, A., Fulop, Z., Gervino, G., Gialanella, L., Guglielmetti, A., Gustavino, C., Imbriani, G., Junker, M., Moroni, P.G., Ordine, A., Prati, P., Roca, V., Rogalla, D., Rolfs, C., Romano, M., Schumann, F., Somorjai, E., Straniero, O., Strieder, F., Terrasi, F., Trautvetter, H.P., Zavatarelli, S.: *Nucl. Phys. A* **690**, 790 (2001)
88. Kimura, S., Takigawa, N., Abe, M., Brink, D.M.: *Phys. Rev. C* **022801**(R), 67 (2003)
89. Eichler, J.: *Phys. Rep.* **193**, 165 (1990)

90. Anholt, R., Gould, H.: *Adv. At. Mol. Phys.* **22**, 315 (1986)
91. Belkacem, A., Gould, H., Feinberg, B., Bossingham, R., Meyerhof, W.E.: *Phys. Rev. Lett.* **71**, 1514 (1993)
92. Frank, F.C.: *Nature* **160**, 525 (1947)
93. Sakharov, A.D.: *Otchet Fiz. Inst. Akad. Nauk*, 1 (1948). (in Russian) translated into English in *Muon Catal. Fusion* **4**, 235 (1989)
94. Zel'dovich, Y.B.: *Dokl. Akad. Nauk. SSSR* **95**, 493 (1954)
95. Alvarez, L.W., et al.: *Phys. Rev.* **105**, 1127 (1957)
96. Jackson, J.D.: *Phys. Rev.* **106**, 330 (1957)
97. Cohen, J.S.: Chap. 2. In: Lin, C.D. (ed.) *Review of Fundamental Processes and Applications of Atoms and Ions*, pp. 61–110. World Scientific, Singapore (1993)
98. Ackerbauer, P., Breunlich, W.H., Fuchs, M., Fussy, S., Jeitler, M., Kammel, P., Lauss, B., Marton, J., Prymas, W., Werner, J., Zmeskal, J., Lou, K., Petitjean, C., Baumann, P., Daniel, H., Hartmann, F.J., Schott, W., Vonegidy, T., Wojciechowski, P., Chatellard, D., Egger, J.P., Jeannot, E., Case, T., Crowe, K.M., Sherman, R.H., Markushin, V.: *Hyperfine Interact.* **82**, 243 (1993)
99. Balin, D.V., Baturin, V.N., Chestnov, Y.A., Ilyin, A.I., Kapinos, P.A., Maev, E.M., Petrov, G.E., Petrov, L.B., Semenchuk, G.G., Smirenin, Y.A., Vorobyov, A.A., Voropaev, N.I.: *Muon Catal. Fusion* **5/6**, 163–169 (1991)
100. Baumann, P., Daniel, H., Grunewald, S., Hartmann, F.J., Lipowsky, R., Moser, E., Schott, W., Vonegidy, T., Ackerbauer, P., Breunlich, W.H., Fuchs, M., Jeitler, M., Kammel, P., Marton, J., Nagele, N., Werner, J., Zmeskal, J., Bossy, H., Crowe, K.M., Sherman, R.H., Lou, K., Petitjean, C., Markushin, V.E.: *Phys. Rev. Lett.* **70**, 3720 (1993)
101. Balin, D.V., Ganzha, V.A., Kozlov, S.M., Maev, E.M., Petrov, G.E., Soroka, M.A., Schapkin, G.N., Semenchuk, G.G., Trofimov, V.A., Vasiliev, A.A., Vorobyov, A.A., Voropaev, N.I., Petitjean, C., Gartner, B., Lauss, B., Marton, J., Zmeskal, J., Case, T., Crowe, K.M., Kammel, P., Hartmann, F.J., Faifman, M.P.: *Phys. Part. Nucl.* **42**, 185 (2011)
102. Bom, V.R., Demin, A.M., Demin, D.L., van Eijk, C.W.E., Faifman, M.P., Filchenkov, V.V., Golubkov, A.N., Grafov, N.N., Grishchkin, S.K., Gritsaj, K.I., Klevtsov, V.G., Konin, A.D., Kuryakin, A.V., Medved, S.V., Musyaev, R.K., Perevozchikov, V.V., Rudenko, A.I., Sadetsky, S.M., Vinogradov, Y.I., Yukhimchuk, A.A., Yukhimchuk, S.A., Zinov, V.G., Zlatoustovskii, S.V.: *Zh. Eksp. Theor. Fiz.* **127**, 152 (2005). *Sov. Phys. JETP* **100**, 663 (2005)
103. Bogdanova, L.N., Bom, V.R., Demin, A.M., Demin, D.L., van Eijk, C.W.E., Filchagin, S.V., Filchenkov, V.V., Grafov, N.N., Grishchkin, S.K., Gritsaj, K.I., Konin, A.D., Kuryakin, A.V., Medveda, S.V., Musyaev, R.K., Rudenko, A.I., Tumkin, D.P., Vinogradov, Y.I., Yukhimchuk, A.A., Yukhimchuk, S.A., Zinov, V.G., Zlatoustovskii, S.V.: *Zh. Eksp. Theor. Fiz.* **135**, 242 (2009). *Sov. Phys. JETP* **108**, 216 (2009)
104. Bogdanova, L., Markushin, V.: *Nucl. Phys. A* **508**, 29c (1990)
105. Bogdanova, L.N., Demin, D.L., Duginov, V.N., Filchenkov, V.V., Gritsaj, K.I., Konin, A.D., Mamedov, T.N., Rudenko, A.I., Stolupin, V.A., Vinogradov, Y.I., Volnykh, V.P., Yukhimchuk, A.A.: *Phys. Part. Nucl. Lett.* **9**, 605 (2012)
106. Breunlich, W.H., Kammel, P., Cohen, J.S., Leon, M.: *Ann. Rev. Nucl. Part. Sci.* **39**, 311 (1989)
107. Gershtein, S.S., Petrov, Y.V., Ponomarev, L.I.: *Usp. Fiz. Nauk* **160**, 3 (1990). *Sov. Phys. Usp.* **33**, 591 (1990)
108. Froelich, P.: *Adv. Phys.* **41**, 405 (1992)
109. Petitjean, C.: *Nucl. Phys. A* **543**, 79 (1992)
110. Nagamine, K.: *Introductory Muon Science*. University Press, Cambridge (2007)
111. Cohen, J.S.: *Rep. Prog. Phys.* **67**, 1769 (2004)
112. Haff, P.K., Tombrello, T.A.: *Ann. Phys.* **86**, 178 (1974)
113. Wightman, A.S.: *Phys. Rev.* **77**, 521 (1950)
114. Cohen, J.S.: *Proceedings of the International School of Physics of Exotic Atoms, 5th Course, Erice, Sicily, 1989*. In: Simons, L.M., Horvath, D., Torelli, G. (eds.) *Electromagnetic Cascade and Chemistry of Exotic Atoms*, pp. 1–22. Plenum, New York (1990)
115. Cohen, J.S.: *Phys. Rev. A* **27**, 167 (1983)
116. Cohen, J.S., Martin, R.L., Wadt, W.R.: *Phys. Rev. A* **24**, 33 (1981)
117. Cohen, J.S., Martin, R.L., Wadt, W.R.: *Phys. Rev. A* **27**, 1821 (1983)
118. Garcia, J.D., Kwong, N.H., Cohen, J.S.: *Phys. Rev. A* **35**, 4068 (1987)
119. Kwong, N.H., Garcia, J.D., Cohen, J.S.: *J. Phys. B* **22**, L633 (1989)
120. Sakimoto, K.: *Phys. Rev. A* **66**, 032506 (2002)
121. Tong, X.M., Shirahama, T., Hino, K., Tushima, N.: *Phys. Rev. A* **75**, 052711 (2007)
122. Fermi, E., Teller, E.: *Phys. Rev.* **72**, 406 (1947)
123. Sakimoto, K.: *Phys. Rev. A* **81**, 012511 (2010)
124. Cohen, J.S.: *Phys. Rev. A* **59**, 1160 (1999)
125. Markushin, V.E.: *Hyperfine Interact.* **119**, 11 (1999)
126. Czaplinski, W., Gula, A., Kravtsov, A., Mikhailov, A., Popov, N.: *Phys. Rev. A* **50**, 525 (1994)
127. Pohl, R., Biraben, F., Conde, C.A.N., Donche-Gay, C., Haensch, T.W., Hartmann, F.J., Hauser, P., Hughes, V.W., Huot, O., Indelicato, P., Knowles, P.E., Kottmann, F., Liu, Y.-W., Markushin, V.E., Mulhauser, F., Nez, F., Petitjean, C., Rabinowitz, P., dos Santos, J.M.F., Schaller, L.A., Schnewly, H., Schott, W., Taqqu, D., Veloso, J.F.C.A.: *Lecture Notes in Physics* vol. 570. Springer, Berlin, p 454 (2001)
128. Jensen, T.S., Markushin, V.E.: *Lecture Notes in Physics* vol. 627. Springer, Berlin, p 37 (2003)
129. Froelich, P., Wallenius, J.: *Phys. Rev. Lett.* **75**, 2108 (1995)
130. Cohen, J.S.: *Phys. Rev. A* **43**, 4668 (1991)
131. Vesman, E.A.: *Pis'ma Zh. Eksp. Fiz.* **5**, 113 (1967). *JETP Lett.* **5**, 91 (1967)
132. Cohen, J.S., Martin, R.L.: *Phys. Rev. Lett.* **53**, 738 (1984)
133. Faifman, M.P., Strizh, T.A., Armour, E.A.G., Harston, M.R.: *Hyperfine Interact.* **101/102**, 179 (1996)
134. Faifman, M.P., Menshikov, L.I., Strizh, T.A.: *Muon Catal. Fusion* **4**, 1 (1989)
135. Leon, M.: *Phys. Rev. Lett.* **52**, 605 (1984)
136. Y.V. Petrov: *Phys. Lett. B* **163**, 28 (1985)
137. Menshikov, L.I., Ponomarev, L.I.: *Phys. Lett. B* **167**, 141 (1986)
138. Cohen, J.S., Leon, M.: *Phys. Rev. A* **39**, 946 (1989)
139. Leon, M.: *Phys. Rev. A* **39**, 5554 (1989)
140. Toyoda, A., Ishida, K., Shimomura, K., Nakamura, S.N., Matsuda, Y., Higemoto, W., Matsuzaki, T., Nagamine, K.: *Phys. Rev. Lett.* **90**, 23401 (2003)
141. Imao, H., Ishida, K., Kawamura, N., Matsuzaki, T., Matsuda, Y., Toyoda, A., Strasser, P., Iwasaki, M., Nagamine, K.: *Phys. Lett. B* **658**, 120 (2008)
142. Fujiwara, M.C., Adamczak, A., Bailey, J.M., Beer, G.A., Beveridge, J.L., Faifman, M.P., Huber, T.M., Kammel, P., Kim, S.K., Knowles, P.E., Kunselman, A.R., Maier, M., Markushin, V.E., Marshall, G.M., Martoff, C.J., Mason, G.R., Mulhauser, F., Olin, A., Petitjean, C., Porcelli, T.A., Wozniak, J., Zmeskal, J.: *Phys. Rev. Lett.* **85**, 1642 (2000)
143. Bystritsky, V.M., Dzhelepov, V.P., Ershova, Z.V., Filchenkov, V.V., Kapyshev, V.K., Mukhamet-Galeeva, S.M., Nadezhdin, V.S., Rivkis, L.A., Rudenko, A.I., Satarov, V.I., Sergeeva, N.V., Somov, L.N., Stolupin, V.A., Zinov, V.G.: *Phys. Lett. B* **94**, 476 (1980)
144. Bogdanova, L.N.: *Muon Catal. Fusion* **3**, 359 (1988)
145. Bogdanova, L.N., Markushin, V.E., Melezhi, V.S., Ponomarev, L.I.: *Yad. Phys.* **34**, 1191 (1981). *Sov. J. Nucl. Phys.* **34**, 662 (1981)



146. Kamimura, M.: In: Jones, S.E., Rafelski, J., Monkhorst, H.J. (eds.) AIP Conference Proceedings 181, Muon-Catalyzed Fusion, p. 330. AIP, New York (1989)
147. Struensee, M.C., Hale, G.M., Pack, R.T., Cohen, J.S.: Phys. Rev. A **37**, 340 (1988)
148. Szalewicz, K., Jeziorski, B., Scrinzi, A., Zhao, X., Moszynski, R., Kolos, W., Froelich, P., Monkhorst, H.J., Velenik, A.: Phys. Rev. A **42**, 3768 (1990)
149. Hu, C.-Y., Hale, G.M., Cohen, J.S.: Phys. Rev. A **49**, 4481 (1994)
150. Hale, G.M.: Muon Catal. Fusion **5/6**, 227–229 (1991)
151. Bracci, L., Fiorentini, G.: Nucl. Phys. A **364**, 383 (1981)
152. Haywood, S.E., Monkhorst, H.J., Szalewicz, K.: Phys. Rev. A **37**, 3393 (1988)
153. Haywood, S.E., Monkhorst, H.J., Alexander, S.A.: Phys. Rev. A **43**, 5847 (1991)
154. Jeziorski, B., Szalewicz, K., Scrinzi, A., Zhao, X., Moszynski, R., Kolos, W., Velenik, A.: Phys. Rev. A **43**, 1640 (1991)
155. Jones, S.E., Anderson, A.N., Caffrey, A.J., Vansiclen, C.D., Watts, K.D., Bradbury, J.N., Cohen, J.S., Gram, P.A.M., Leon, M., Maltrud, H.R., Paciotti, M.A.: Phys. Rev. Lett. **56**, 588 (1986)
156. Breunlich, W.H., Cargnelli, M., Kammel, P., Marton, J., Naegele, N., Pawlek, P., Scrinzi, A., Werner, J., Zmeskal, J., Bistirlich, J., Crowe, K.M., Justice, M., Kurck, J., Petitjean, C., Sherman, R.H., Bossy, H., Daniel, H., Hartmann, F.J., Neumann, W., Schmidt, G.: Phys. Rev. Lett. **58**, 329 (1987)
157. Nagamine, K., Matsuzaki, T., Ishida, K., Hirata, Y., Watanabe, Y., Kadono, R., Miyake, Y., Nishiyama, K., Jones, S.E., Maltrud, H.R.: Muon Catal. Fusion **1**, 137 (1987)
158. Froelich, P., Flores-Riveros, A.: Phys. Rev. Lett. **70**, 1595 (1993)
159. Kawamura, N., Nagamine, K., Matsuzaki, T., Ishida, K., Nakamura, S.N., Matsuda, Y., Tanase, M., Kato, M., Sugai, H., Kudo, K., Takeda, N., Eaton, G.H.: Phys. Rev. Lett. **90**, 043401 (2003)
160. Baluev, V.V., Bogdanova, L.N., Bom, V.R., Demin, D.L., van Eijk, C.W.E., Filchenkov, V.V., Grafov, N.N., Grishechkin, S.K., Gritsaj, K.I., Konin, A.D., Mikhailuykov, K.L., Rudenko, A.I., Vinogradov, Y.I., Volnykh, V.P., Yukhimchuk, A.A., Yukhimchuk, S.A.: Zh. Eksp. Theor. Fiz. **140**, 80 (2011). Sov. Phys. JETP **113**, 68 (2011)
161. Petrov, Y.V.: Nature **285**, 466 (1980)
162. Petrov, Y.V.: Muon Catal. Fusion **3**, 525 (1988)
163. Kase, T., Konashi, K., Sasao, N., Takahashi, H., Hirao, Y.: Muon Catal. Fusion **5/6**, 521–529 (1991)
164. Anisimov, V.V., Arkhangel'sky, V.A., Ganchuk, N.S., Yukhimchuk, A.A., Cavalleri, E., Karmanov, F.I., Konobeyev, Y.A., Slobodtchouk, V.I., Latysheva, L.N., Pshenichnov, I.A., Ponomarev, L.I., Vecchi, M.: Fusion Technol. **39**, 198 (2001)
165. Jones, S.E., Taylor, S.F., Anderson, A.N.: Hyperfine Interact. **82**, 303 (1993)
166. Petitjean, C., Balin, D.V., Baturin, V.N., Baumann, P., Breunlich, W.H., Case, T., Crowe, K.M., Daniel, H., Grigoriev, Y.S., Hartmann, F.J., Ilyin, A.I., Jeitler, M., Kammel, P., Lauss, B., Lou, K., Maev, E.M., Marton, J., Muhlbauer, M., Petrov, G.E., Prymas, W., Schott, W., Semenchuk, G.G., Smirenin, Y.V., Vorobyov, A.A., Voropaev, N.I., Wojciechowski, P., Zmeskal, J.: Hyperfine Interact. **82**, 273 (1993)
167. Nagamine, K., Ishida, K., Sakamoto, S., Watanabe, Y., Matsuzaki, T.: Hyperfine Interact. **82**, 343 (1993)
168. Ishida, K., Nagamine, K., Matsuzaki, T., Kawamura, N., Nakamura, S.N., Matsuda, Y., Kato, M., Sugai, H., Tanase, M., Kudo, K., Takeda, N., Eaton, G.H.: Hyperfine Interact. **138**, 225 (2001)
169. Bossy, H., Daniel, H., Hartmann, F.J., Neumann, W., Plendl, H.S., Schmidt, G., Vonegidy, T., Breunlich, W.H., Cargnelli, M., Kammel, P., Marton, J., Naegele, N., Scrinzi, A., Werner, J., Zmeskal, J., Petitjean, C.: Phys. Rev. Lett. **59**, 2864 (1987)
170. Paciotti, M.A., Baker, O.K., Bradbury, J.N., Cohen, J.S., Leon, M., Maltrud, H.R., Sturgess, L.L., Jones, S.E., Li, P., Rees, L.M., Sheely, E.V., Shurtleff, J.K., Taylor, S.F., Anderson, A.N., Caffrey, A.J., Zabriskie, J.M., Brooks, F.D., Cilliers, W.A., Davies, J.D., England, J.B.A., Pyle, G.J., Squier, G.T.A., Bertin, A., Bruschi, M., Piccinini, M., Vitale, A., Zoccoli, A., Bom, V.R., van Eijk, C.W.E., de Haan, H., Eaton, G.H.: In: Jones, S.E., Rafelski, J., Monkhorst, H.J. (eds.) AIP Conference Proceedings 181, Muon-Catalyzed Fusion, p. 38. AIP, New York (1989)
171. Case, T., Crowe, K.M., Lou, K., Petitjean, C., Breunlich, W.H., Jeitler, M., Kammel, P., Lauss, B., Marton, J., Prymas, W., Zmeskal, J., Balin, D.V., Baturin, V.N., Grigoriev, Y.S., Ilyin, A.I., Maev, E.M., Petrov, G.E., Semenchuk, G.G., Smirenin, Y.V., Vorobyov, A.A., Voropaev, N.I., Baumann, P., Daniel, H., Hartmann, F.J., Muhlbauer, M., Schott, W., Wojciechowski, P.: Hyperfine Interact. **82**, 295 (1993)
172. Struensee, M.C., Cohen, J.S.: Phys. Rev. A **38**, 44 (1988)
173. Stodden, C.D., Monkhorst, H.J., Szalewicz, K., Winter, T.G.: Phys. Rev. A **41**, 1281 (1990)



**James S. Cohen** Dr Cohen is Group Leader of the Atomic and Optical Theory Group in the Theoretical Division of Los Alamos National Laboratory and a Fellow of the American Physical Society. He received a PhD in Physics from Rice University in 1973. His general area of research is theoretical atomic and molecular physics, with a special interest in exotic muonic and antiprotonic species.



**John D. Morgan III** Dr Morgan, Associate Professor, obtained his BS from The George Washington University, his MSc in Theoretical Chemistry from Oxford University, and his PhD in Chemistry from Berkeley. He has served on the editorial boards of the *Journal of Mathematical Physics* and the *International Journal of Quantum Chemistry*. His interests include the application of sophisticated mathematical techniques to assist the accurate calculation of properties of atoms and molecules.